Research article

PG
Petroleum Geoscience

https://doi.org/10.1144/petgeo2022-021 | Vol. 29 | 2023 | petgeo2022-021

Rock mechanical properties of immature, organic-rich source rocks and their relationships to rock composition and lithofacies

Israa S Abu-Mahfouz[1]*, Regina Iakusheva[2,‡], Thomas Finkbeiner[2], Joe Cartwright[3] and Volker Vahrenkamp[2]

[1] Department of Geosciences, College of Petroleum Engineering & Geosciences, King Fahd University of Petroleum and Minerals, Dhahran 34463, Saudi Arabia
[2] Ali I. Al-Naimi Petroleum Engineering Research Center, King Abdullah University of Science and Technology, Thuwal, Saudi Arabia
[3] Department of Earth Sciences, University of Oxford, South Parks Road, Oxford OX1 3AN Oxford, UK
[‡] Co-first author
ISA, 0000-0001-5832-7354
* Correspondence: israa.abumahfouz@kfupm.edu.sa

Abstract: Mechanical properties of layered rocks are critical in ensuring wellbore integrity and predicting natural fracture occurrence for successful reservoir development, particularly in unconventional reservoirs for which fractures provide the main pathway for hydrocarbon flow. We examine rock mechanical properties of exceptionally organic-rich, immature source rocks from Jordan, and understand their relationships with rock mineral composition and lithofacies variations. Four depositional microfacies were identified: organic-rich mudstone, organic-rich wackestone, silica-rich packstone and fine-grained organic-rich wackestone. The four types exhibit various mineralogical compositions, dominated by carbonates, biogenic quartz and apatite. Leeb hardness ranges between 288 and 654, with the highest average values occurring in silica-rich packstone and organic-rich mudstone. The highest uniaxial compressive strength (derived from the intrinsic specific energy measured using an Epslog Wombat scratch device), and compressional- and shear-wave velocities were measured in organic-rich mudstones (140 MPa, 3368 m s^{-1} and 1702 m s^{-1}, respectively). Porosity shows higher average values in organic-rich wackestones and fine-grained organic-rich wackestones (33–35%). Silica-rich packstone and organic-rich mudstone have brittle properties, while organic-rich wackestone and fine-grained organic-rich wackestone are ductile. High silica contents are correlated positively with brittleness. A strong hardness–brittleness correlation suggests that Leeb hardness is a useful proxy for brittleness. Our study allows a better understanding of the relationships between lithofacies, organic content and rock mechanical properties, with implications for fracking design to well completion and hydrocarbon production. Further work involving systematic sampling and a more rigorous study is still required to better understand the spatial distribution of target lithologies and their mechanical properties.

Received 22 March 2022; **revised** 6 December 2022; **accepted** 6 January 2023

During the last century, the growth of energy needs has led to decades of extensive oil and gas production from conventional hydrocarbon resources. Declining growth rates of traditional oil resources, coupled with continued growth in world energy consumption, led, in the late 1990s, to alternative hydrocarbon sources being considered (Abu-Hamatteh *et al.* 2008). From the early 2000s, technical developments that were mainly related to drilling and reservoir stimulation allowed huge oil and gas volumes trapped in tight source rocks, which became known as 'unconventional' reservoirs, to be unlocked (Council 2016).

Organic-rich oil shale resources/source rocks of different compositions, which are abundant and described in 27 countries on all continents, are considered as important unconventional hydrocarbon plays. Hydrocarbon volumes assigned to these combined unconventional resources are estimated to be four times the size of the world's conventional crude oil resource (Speight 2019). However, regardless of rock composition and depositional origin, unconventional hydrocarbon plays are generally characterized by their low porosities (<10%), ultra-low permeabilities (< mD) and poor connectivity (Zou *et al.* 2012; Gensterblum *et al.* 2015; Aguilera 2016).

Rock mechanical properties, including rock strength, hardness, brittleness and elastic moduli, are considered to be some of the most important factors controlling the response of unconventional reservoirs to the generation of natural fractures and artificial stimulation through hydraulic fracturing. Hence, it is crucial to understand how the mechanical properties of rocks change in different lithologies. Many researchers have examined the relationship between rock mechanical properties and mineralogical characteristics of various formations with different compositions. For example, some studies have found an increase of rock compressive strength with increasing concentrations of specific types of minerals, such as quartz (e.g. Gunsallus and Kulhawy 1984; Brunhoeber *et al.* 2020). Hugman and Friedman (1979) and Eberli *et al.* (2003) reported that both the ultimate strength of rocks and the sonic velocity rise with an increased content of dolomite and microcrystalline carbonate. Horsund (2001) reported some correlations between P-wave velocity, uniaxial compressive strength (UCS) and Young's modulus (YM) that can be used for the prediction of shale mechanical properties.

Brunhoeber *et al.* (2020) concluded that porosity is related to a rock's mechanical properties, in that the UCS increases with a reduction in porosity. Ajalloeian *et al.* (2017) showed that the rock strength and Young's modulus of packstones are less than those found in wackestones due to a higher allochem content and a higher percentage of intraparticle porosity in packstones. Fjær *et al.* (2008) documented that the elastic properties of bulk rocks mainly depend on the relative amount, the geometrical distribution and the elastic properties of each constituent.

The present study investigates the rock mechanical, petrophysical and geochemical characteristics of the Upper Cretaceous organic-

rich carbonate mudrocks of Jordan, colloquially known as the Jordan oil shale (JOS). These rocks are widely distributed across Jordan, underlying more than 60% of the territory (Alali 2006). JOS is composed predominantly of carbonates (Huggett *et al.* 2017) and has a low thermal maturity, which would require artificial heating to generate oil (Hakimi *et al.* 2016; Abu-Mahfouz *et al.* 2019, 2022*a*, *b*; Grohmann *et al.* 2021).

The Upper Cretaceous source rocks of Jordan have previously been studied for their stratigraphy and sedimentology (e.g. Quennell 1951; Burdon 1959; Bender 1968; Powell 1989; Amireh 1996; Baaske 2005; Powell and Moh'd 2011, 2012; Bandel and Salameh 2013), depositional environment, biostratigraphy and geochemistry (e.g. Alqudah *et al.* 2014, 2015; Ali Hussein *et al.* 2015; Hakimi *et al.* 2016), diagenesis (e.g. Huggett *et al.* 2017), and structures (e.g. Hooker and Cartwright 2016; Hooker *et al.* 2017, 2019; Abu-Mahfouz *et al.* 2019, 2020*a*, *b*, 2022*a*, *b*; Wicaksono *et al.* 2022). However, there is a lack of studies focusing on the rock mechanical properties of these Upper Cretaceous source rocks. Thus, this study mainly aims at answering the following questions: (1) What are the mechanical properties (uniaxial compressive strength, Leeb hardness and brittleness) of the Upper Cretaceous source rocks of Jordan? (2) What impact do compositional and facies variations have on rock mechanical properties? (3) How does the occurrence and distribution of organic matter influence the mechanical properties of rocks?

This detailed rock mechanical evaluation will help to: (1) assess the potential of unconventional source rocks as a resource; (2) build reservoir models that more accurately reflect the compositional and mechanical heterogeneities of a reservoir; (3) potentially lead to improved stimulation techniques and production of hydrocarbons; and (4) contribute to a better understanding of mature unconventional source-rock analogue sequences elsewhere.

Geological settings

Jordan is located in the northwestern part of the Arabian Peninsula and bordered to the west by the Dead Sea Rift Valley. During the Late Cretaceous–Eocene, Jordan was situated at the southern margin of the Neo-Tethys Ocean, which periodically transgressed to the south and east onto the Arabic Craton, transforming the area into a broad, shallow-marine, outer continental shelf (Fig. 1a, b). Post-rift flexural subsidence of the continental margin lasted from the Cenomanian to the Eocene, leading to more than 1 km of carbonate material being deposited in the northern part of Jordan, with reduced thickness to the south and SE of the country (Powell and Moh'd 2011). However, this period was terminated by the collision of the Afro-Arabian and the Eurasian plates, leading to uplift, folding and erosion in the latest Eocene (Lovelock 1984; Powell 1989; Butterlin *et al.* 1993; Abed *et al.* 2005; Diabat and Masri 2005; Haq and Qahtani 2005; Lopes and Cunha 2007).

Abed *et al.* (2005) and Alqudah *et al.* (2015) proposed a model for the accumulation of organic matter in small sub-basins, which were formed due to the differential subsidence of graben and half-graben systems bounded by the major faults. JOS accumulated in these tectonically controlled intra-shelf basins, which were characterized by dysaerobic and anoxic reducing conditions, and

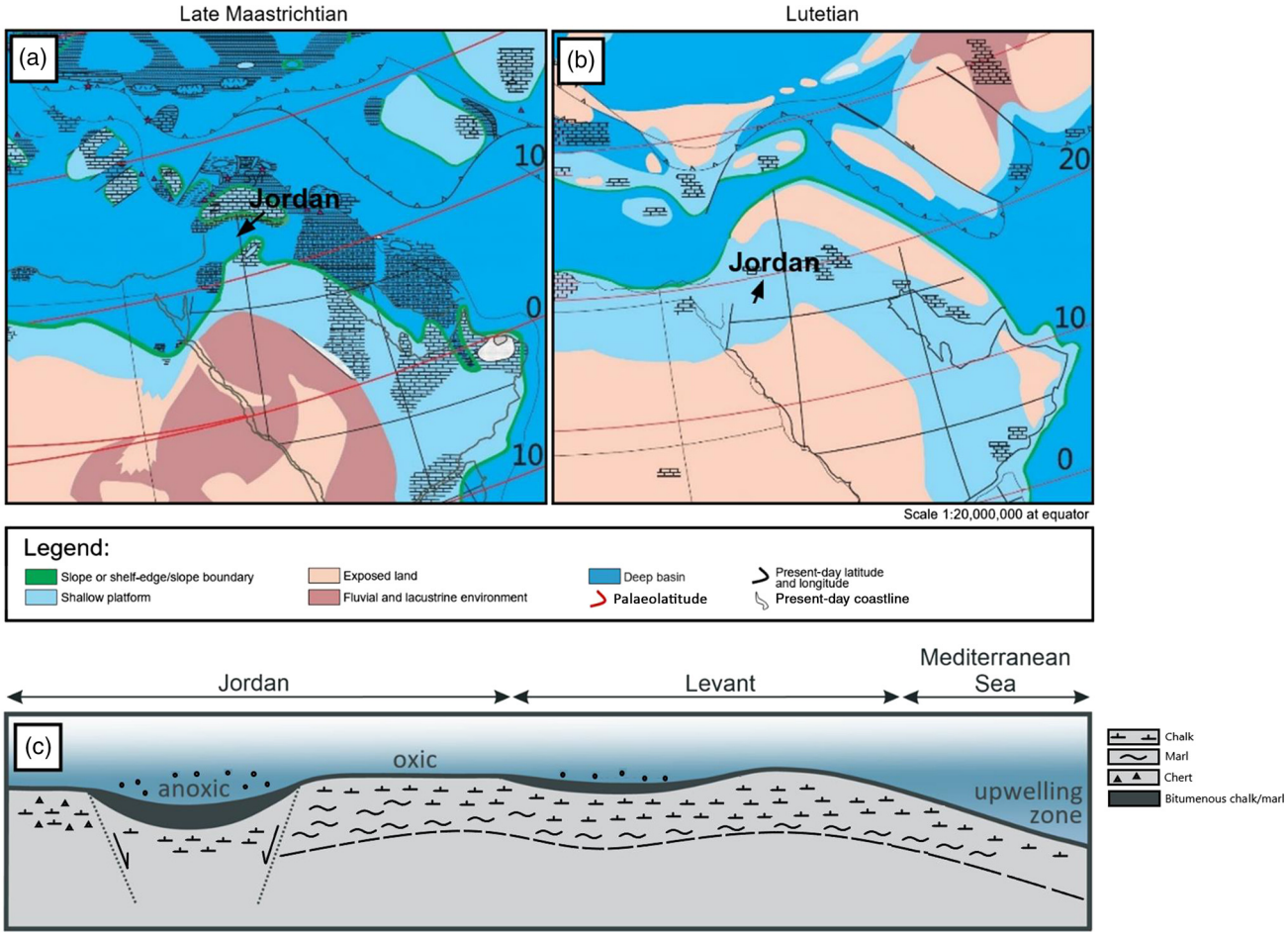

Fig. 1. (**a**) and (**b**) Palaeogeographical map of Jordan (Maastrichtian–Eocene time) (from Alqudah *et al.* 2015; Eocene map modified from Butterlin *et al.* 1993). Schematic depositional settings of the Maastrichtian–Tertiary depositional sequence. (**c**) ESE–WNW cross-section across Jordan and Levant (modified from Powell and Moh'd 2011). See the map in Figure 3 for the cross-section outline (outlined in red).

a high bioproductivity regime. This high bioproductivity was controlled by the upwelling of nutrient-rich currents (Fig. 1c) (Almogi-Labin *et al.* 1993; Powell and Moh'd 2011; Abed 2013).

The study interval comprises the organic-rich Upper Cretaceous source rocks deposited during the Maastrichtian–Paleocene. This organic-rich interval is represented by the Maastrichtian Muwaqqar Chalk Marl Formation (MCM), which overlies the Upper Campanian–Lower Maastrichtian Al-Hisha Phosphorite Formation (AHP) and hosts exceptionally organic-rich carbonate mudrocks (Alqudah *et al.* 2015; Abu-Mahfouz *et al.* 2019).

The thickness of the MCM formation ranges from a few tens of metres in the south to more than 750 m in the Sirhan Sub-basin (Alqudah *et al.* 2015), and typically consists of organic-rich chalk and chalky marl, argillaceous chalky limestone, limestone with concretions of chert and, locally, microcrystalline limestone (Ali Hussein *et al.* 2014) (Fig. 2). Fossils observed in this formation are represented by bivalves, ammonites, gastropods, fish fragments and calcareous nanoplankton (Powell and Moh'd 2011).

Materials and methods

Dataset

Twenty-one samples for this study were extracted from cores retrieved from 12 vertical wells drilled into the Upper Cretaceous strata located in different sub-basins across Jordan. One core was extracted from the Yarmouk Sub-basin (northern Jordan), four cores from the Azraq-Hamza Sub-basin (central east Jordan), one from the Sirhan Sub-basin (southern east Jordan), three from the Jafr Sub-basin (southern Jordan) and three from the Lajjun Sub-basin (central Jordan) (Fig. 3). These samples were selected to reflect the variety of mineral composition and depths, which ranged from 80.5 to 875 m (Fig. 4).

Microscopic investigation

Seventeen thin sections (30 µm thick) were microscopically investigated for their composition, texture and microfacies using a Leica ICC50W optical microscope. Ten representative thin sections were selected for the scanning electron microscopy/energy dispersive spectroscopy (SEM/EDS) examination using a FEI Teneo VolumeScope System. The characterization of skeletal grains, types of intraclasts, grain preservation, compaction, type of cement, presence of organic matter, microfractures, pore networks and grain distribution were important in the microfacies classification.

Geochemical analyses

X-ray diffraction (XRD) analysis is a fundamental mineral identification tool used by mineralogists to recognize the mineralogical composition from angles and intensities of observable diffraction peaks (Lavina *et al.* 2014). A Bruker D2 Phaser diffractometer was used to conduct the XRD analysis on powdered samples with a size of 1–50 µm. Each sample was checked for 14 minerals (calcite, calcium magnesium carbonate, fluorapatite, apatite, dolomite, quartz, illite, montmorillonite, kaolinite, smectite, gypsum, goethite, ankerite and pyrite) that are likely to occur in the study source-rocks interval (Abed and Amireh 1983; Jaber *et al.* 2011; Alnawafleh *et al.* 2016; Gharaibeh 2017; Huggett *et al.* 2017; Dhoun and Al-Zyod 2019; Ibrahim *et al.* 2019; Li *et al.* 2019). The abundance and concentration of the minerals were analysed using the database of the Joint Committee Powder Diffraction Standards–International Centre for Diffraction Data (JCPDS–ICDD) 2015.

The total organic carbon (TOC) content, which indicates source-rock richness and the potential volume of hydrocarbon generation (Steiner *et al.* 2016), was measured for 19 selected samples using fully automated Vinci Rock-Eval 6 apparatus.

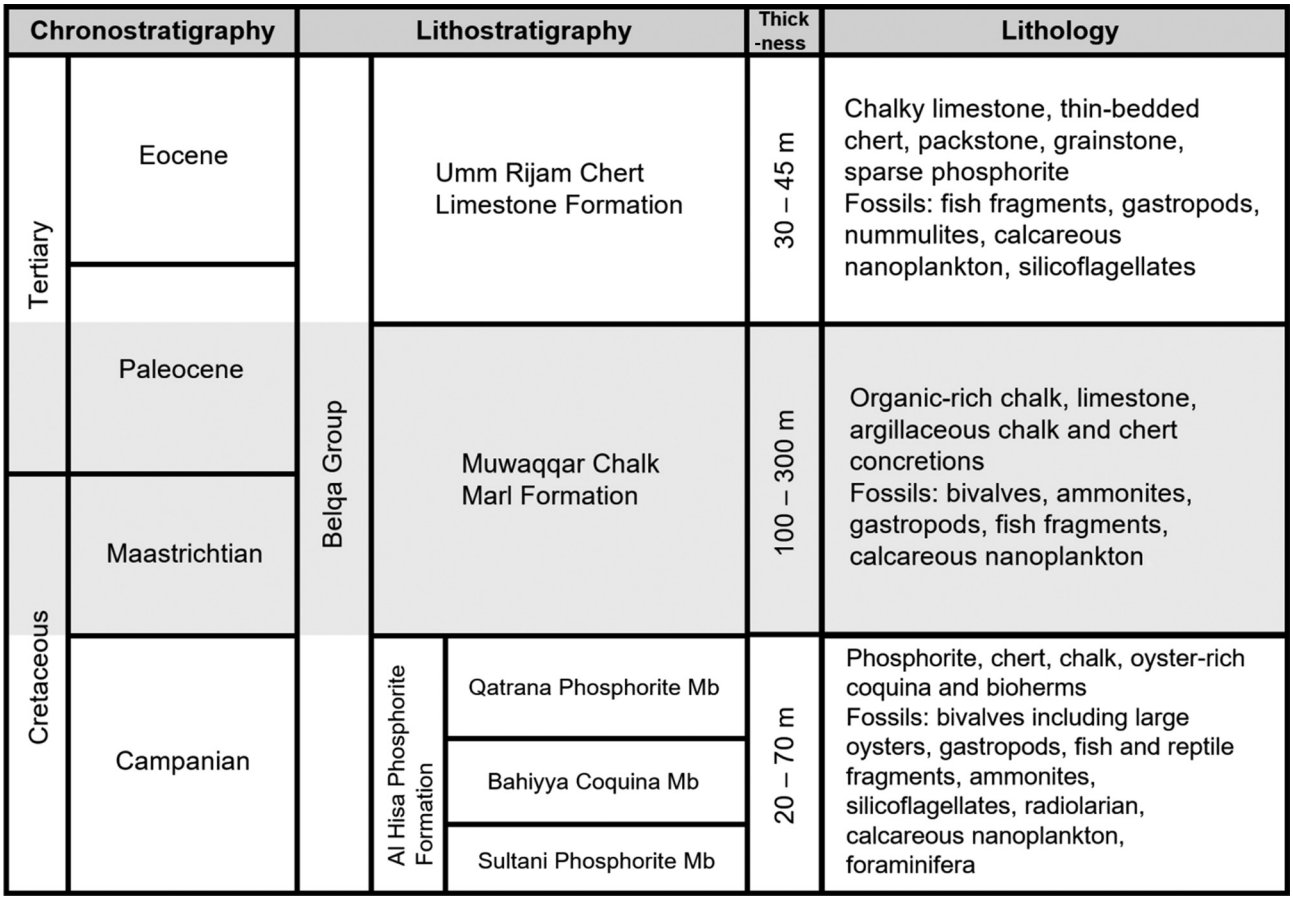

Fig. 2. Chronostratigraphy and lithostratigraphy of central Jordan (modified from Powell and Moh'd 2011).

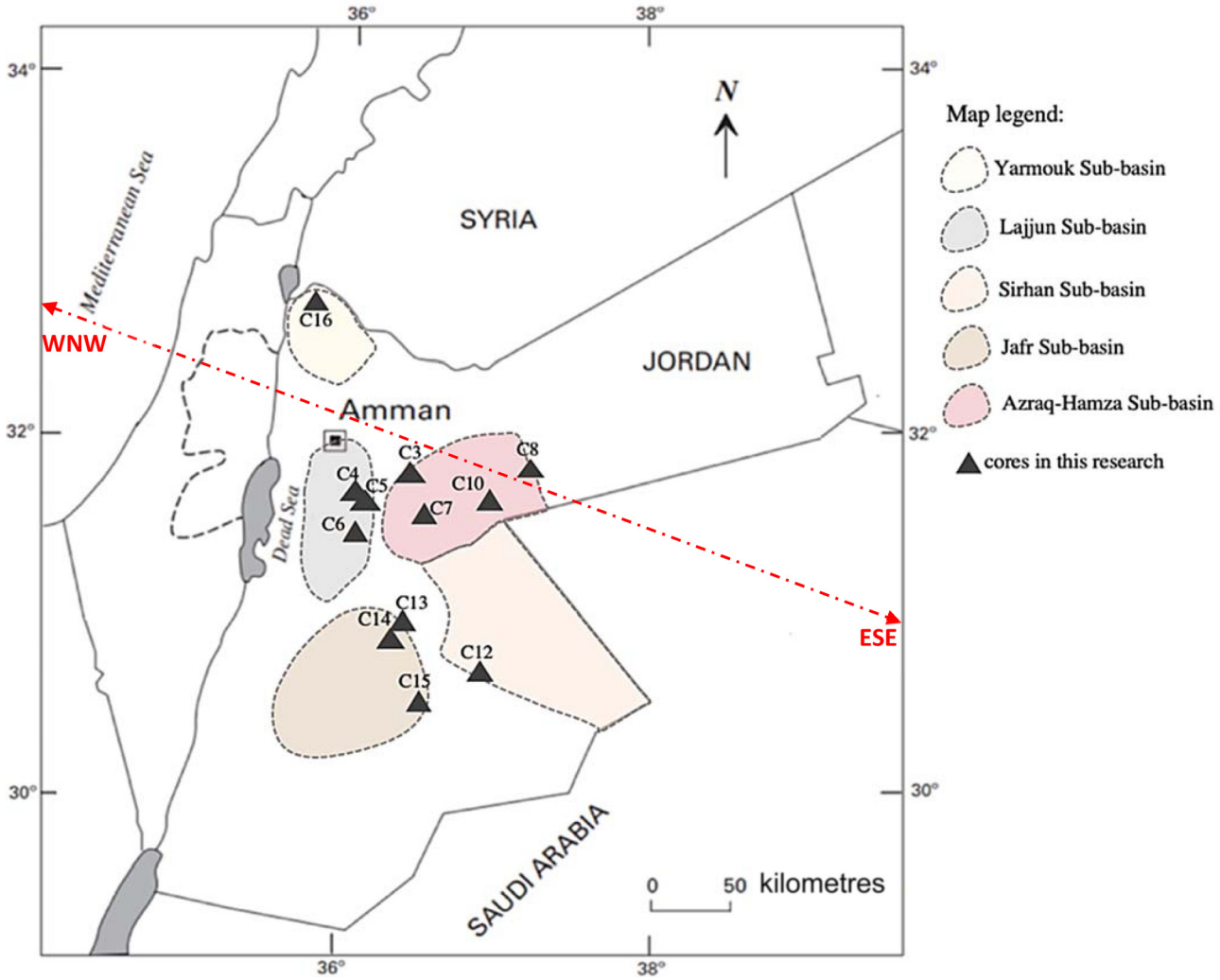

Fig. 3. Location of the vertical wells in Jordan. Dashed-coloured shapes show the five main sub-basins in the country (Jordan oil shale deposits map modified from Dyni 2006; basin outlines modified from Alqudah *et al.* 2015).

Rock mechanical analyses

Rebound hardness tests were performed on core samples placed on a solid support (according to international standards: ASTM 2001) using an Equotip 550 Leeb D portable device. As the variations in the readings are strictly related to the material heterogeneity, a 4 × 4 mm net was created to capture the material differences on the specimen surface, and at least 18 independent readings were obtained for each surface. The rebound hardness measurements were taken at the intersection of the generated squares (Fig. 5). To avoid abnormally low values caused by impact energy dissipation, Leeb hardness (LH) measurements were obtained away from the core edges (Day 1977). Anomalies (exceptionally high and low measurements) were excluded from the analysis and, later, the mean, maximum and minimum values of the selected readings were derived for each sample.

Furthermore, the study specimens were tested using a scratch device (Epslog Wombat) to measure the intrinsic specific energy (ISE), which is defined as the energy required to cut a unit volume of rock. ISE can be calculated using the following equation:

$$\varepsilon = \frac{F - VI}{wd} \quad (1)$$

where F is the force required to cut a unit volume of rock, VI is the vertical intersect, w is the width of the cutter and d is the depth of cut.

The ISE is considered a robust indicator of uniaxial compressive strength (Richard *et al.* 2012; Germay and Richard 2014). Several studies have demonstrated a strong correlation between ISE and UCS (e.g. Schei *et al.* 2000; Dagrain *et al.* 2004; Richard *et al.* 2012; Germay and Richard 2014). Sample preparation for the scratch test is straightforward as it only requires a flat and smooth surface to ensure a fixed position of the rock sample on the horizontal bed.

Despite the interconnection between these two parameters (ISE and UCS), the specimen might be subjected to dissipation and cracking since the UCS values were derived using a scratch device (Epslog Wombat). Thus, the upper 2 mm of the sample surface should be removed before testing. In order to estimate the reliable value of ISE of the tested samples, several scratches (at least five performed in the ductile regime) should be conducted with various depths of cuts before chipping occurs. Other values, which are performed in the brittle mode or in the region where friction is not stabilized, were excluded from the analysis.

Petrophysical analyses

Core plugs, 1 inch in diameter, were tested for porosity using a MetaRock PDP-300 helium porosimeter and by applying Boyle's law to the ideal gas (Noah and Shazly 2014).

Using the Epslog Wombat scratch device, ultrasonic travel times, and derived compressional-wave (v_P) and shear-wave (v_S) velocities were measured in different locations along the core samples. Young's

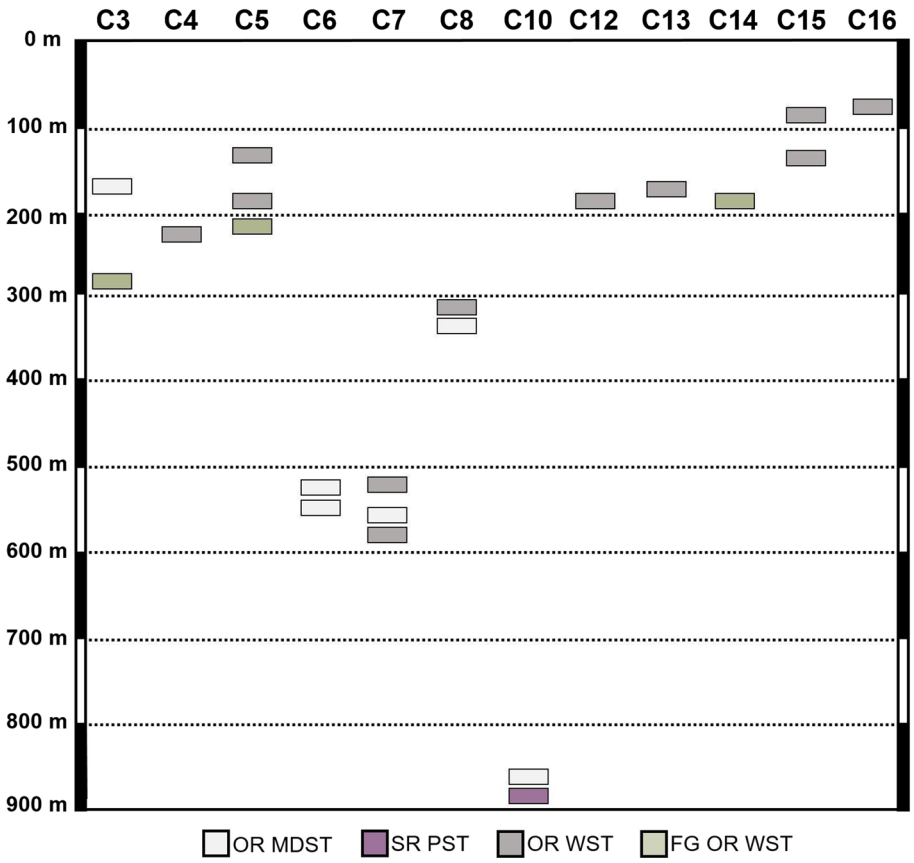

Fig. 4. Figure showing the depth of the study samples collected from the 12 cores and the spatial distributions of the four microfacies defined in the study samples. OR MDST, organic-rich mudstone; SR PST, silica-rich packstone; OR WST, organic-rich wackestone; FG OR WST, fine-grained organic-rich wackestone.

modulus (YM) and Poisson's ratio (PR) were then calculated according to the following equations (Russell and Smith 2007):

$$\mathrm{YM} = \frac{\rho v^2 (3v_\mathrm{P}^2 - 4v_\mathrm{S}^2)}{v_\mathrm{P}^2 - v_\mathrm{S}^2} \quad (2)$$

$$\mathrm{PR} = \frac{v_\mathrm{P}^2 - 2v_\mathrm{S}^2}{2(v_\mathrm{P}^2 - v_\mathrm{S}^2)} \quad (3)$$

Results

Microfacies characteristics

Four major depositional microfacies types of heterogeneous porosity and nanodarcy permeability were identified in this study. These are silica-rich packstone (one sample), organic-rich mudstone (six samples), organic-rich wackestone (11 samples) and fine-grained organic-rich wackestone (three samples):

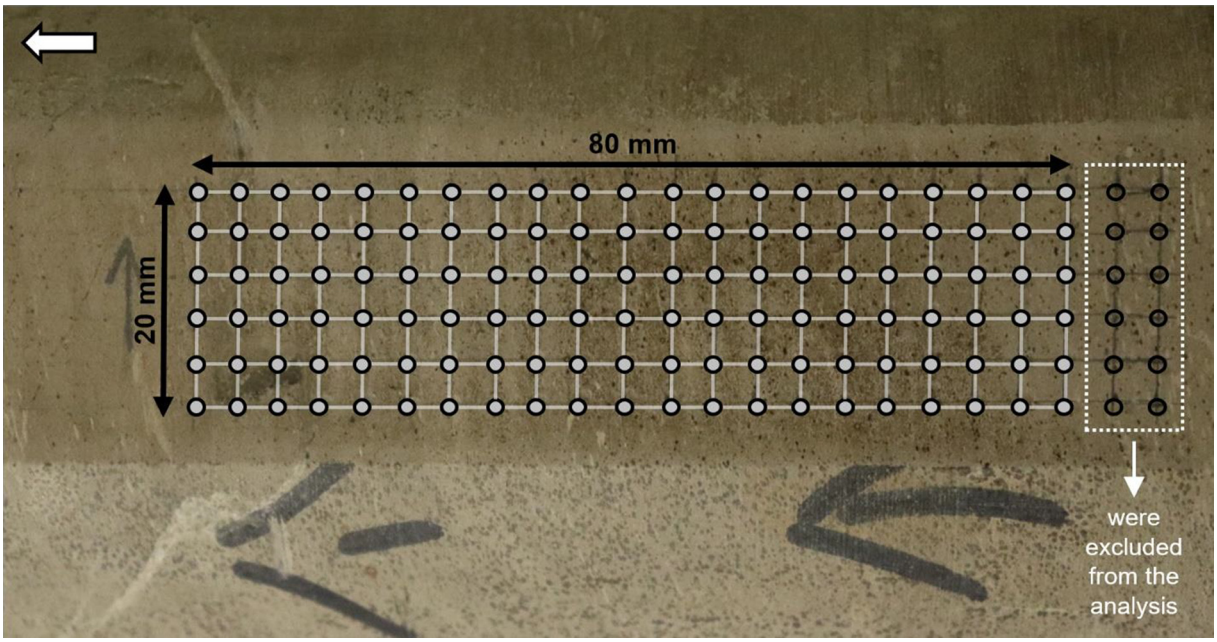

Fig. 5. Representative sample surface, showing the generated net for the rebound hardness test analysis. Very low values (black circles on the right) were excluded from the analysis.

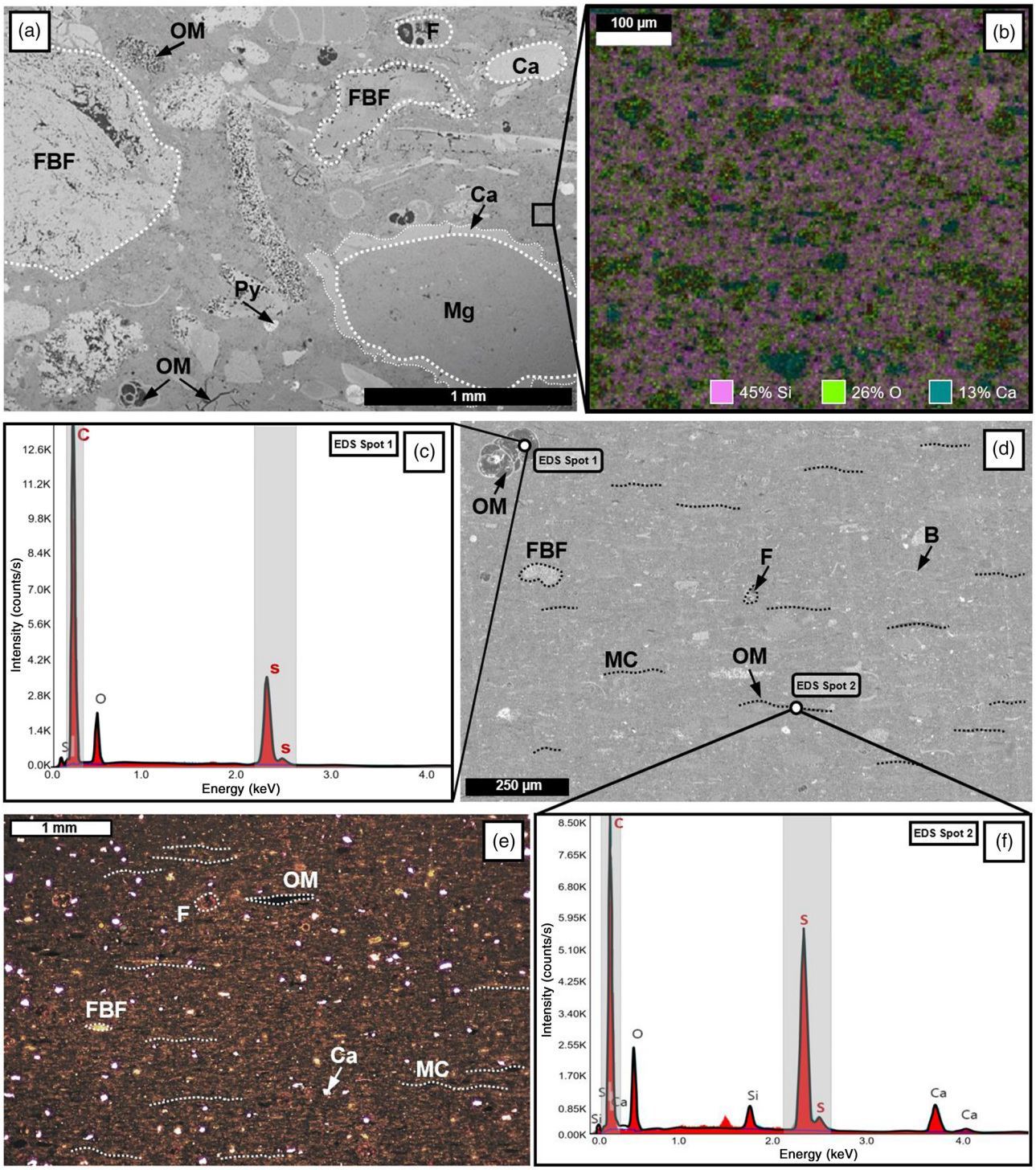

Fig. 6. Thin-section microphotographs and BSE/EDS images showing examples of (**a**) silica-rich packstone, and (**d**) and (**e**) organic-rich mudstone. (**b**) EDS map depicting the siliceous matrix composition of SR PST. (**c**) and (**f**) EDS maps showing the presence of organic matter within foraminifera tests and microcracks. B, bivalve; Ca, calcite grain/rims; F, foraminifera; FBF, fish bone fragment; MC, microcrack; Mg, magnesium-rich grain; OM, organic matter; Py, pyrite.

(1) Silica-rich packstone microfacies (SR PST): black, laminated, poorly sorted Si-rich packstone microfacies (Fig. 6a, b). Intraclasts and bioclasts form 40% of the sample. Fish bone fragments (apatite/fluorapatite) up to 6 mm in size and of various shapes are abundant. Bright pyrite grains and assemblages (15–78 µm in diameter) can be seen in SEM images (Fig. 6a). Tissot and Welte (1984) assumed that pyrite formation is associated with H_2S and free S^{2-} under dysaerobic and anoxic conditions, where the excess sulfur was incorporated into the organic matter or combined with iron. The organic matter content is low compared to other microfacies types and occurs distributed in the matrix, filling microcracks or partially filling some of the foraminifera shells and microcavities in the fish bone fragments. Based on EDS maps, the matrix of this microfacies type is siliceous (Fig. 6b). Most of the foraminifera grains are cemented. Rims of the foraminifera shells are composed of calcite, while the majority of the cement filling the foraminifera shells is dolomite/magnesium-rich calcite. Blocky calcite cement

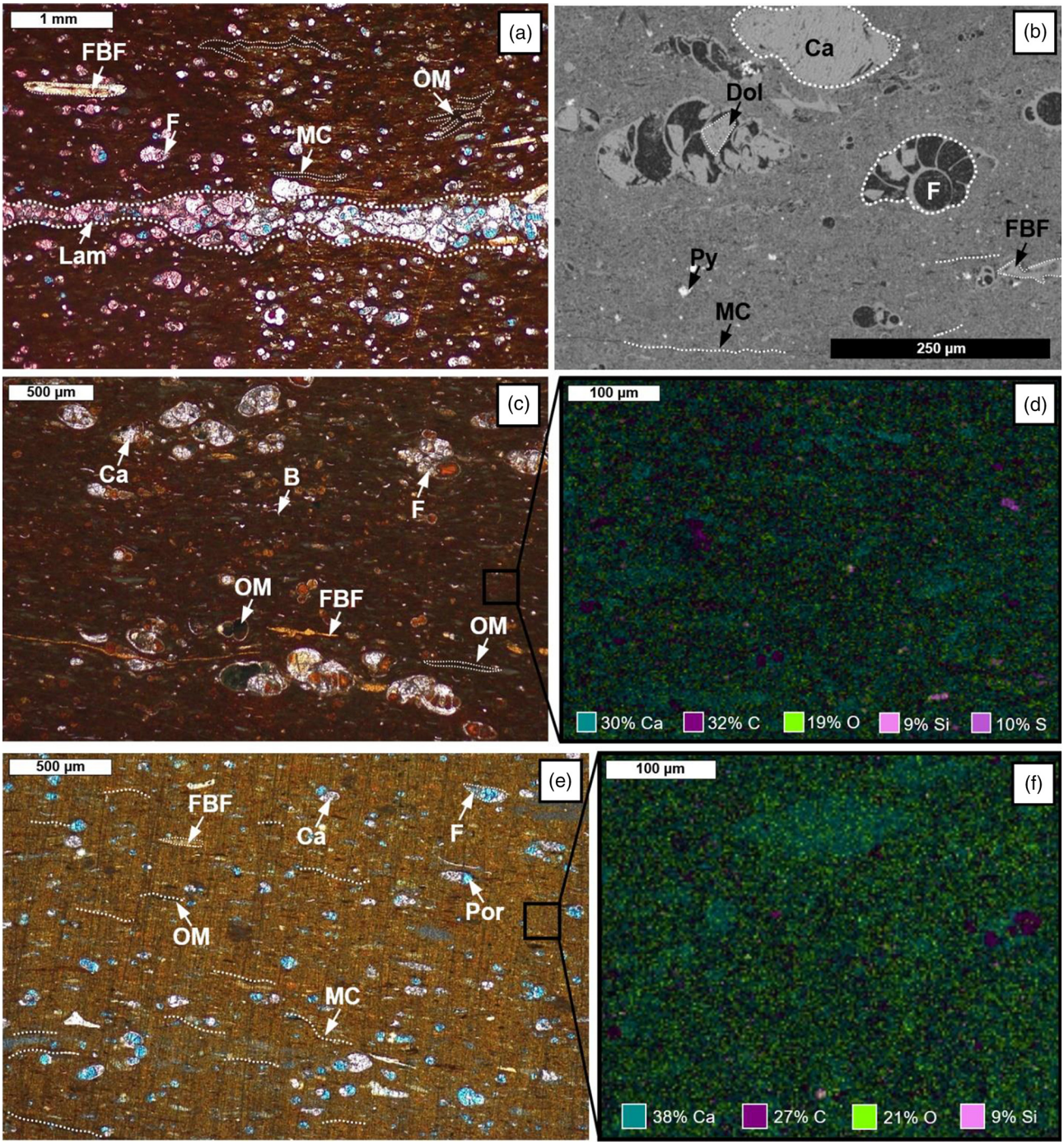

Fig. 7. Thin-section microphotographs and BSE/EDS images showing examples of (**a**)–(**d**) organic-rich wackestone, and (**e**) and (**f**) fine-grained organic-rich wackestone. (d) EDS map depicting the calcareous matrix composition of OR WST. Organic matter is dissipated in the matrix and microcracks. Foraminifera lamina are shown in (a). (a) and (e) Intraparticle porosity is filled with blue epoxy and is relatively high. B, bivalve; Ca, calcite cement; Dol, dolomite crystal; F, foraminifera; FBF, fish bone fragment; Lam, laminae; MC, microcrack; OM, organic matter; Por, intraparticle porosity; Py, pyrite.

occupies the inner part of some of the larger fish bones. Pore size depends on the size of dissolved shell/bone fragments, and ranges between 0.25 and 1 mm.

(2) Organic-rich mudstone microfacies (OR MDST): black laminated, organic-rich mudstone microfacies (Fig. 6c–f). The main components include planktonic foraminifera, with a few benthic types, phosphatic fish bone fragments (up to 4.5 mm) and rare bivalves. Based on the EDS maps, the matrix is mainly siliceous, where calcium exists in the form of lenses (38–190 μm in length). Organic matter is observed to be occupying foraminifera grains (Fig. 6c, d) or filling microcracks in the matrix (Fig. 6d–f). The shape of foraminifera chambers is recognizable and well preserved due to the calcite cementation of the tests. The porosity is not visible.

(3) Organic-rich wackestone microfacies (OR WST): light grey–dark brown, organic-rich, poorly sorted microfacies (Fig. 7a–d). It is the dominant microfacies type (seen in 11 out of 21 samples). Grains are mainly represented by planktonic foraminiferas, bivalves and large fish bone fragments. Bioclasts are often arranged as thin foraminiferal packstone laminae interbedded with a homogenous calcitic matrix, as seen under the SEM (Fig. 7a, c, d). Organic matter generally occurs in three forms: distributed in the matrix, filling foraminifera shells and filling horizontal cracks/fractures of 55–182 μm in length. Several samples

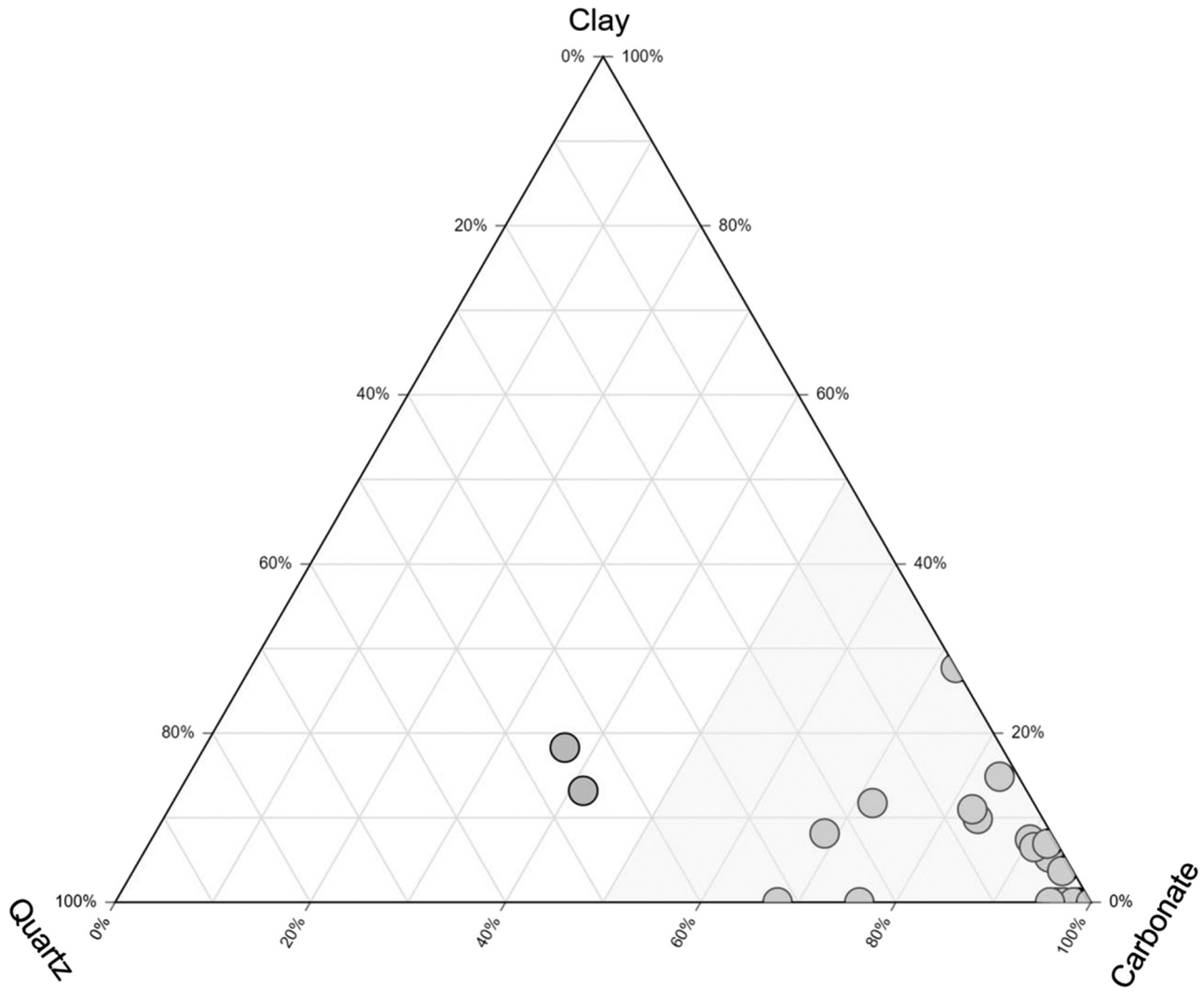

Fig. 8. Ternary plot showing the mineral composition of 21 tested Jordan oil shales. Note that the majority of the samples are exceptionally rich in carbonate.

show high fracture intensity, where some of these fractures are partially cemented by calcite but the majority are filled with organic matter. Calcite rim cement is present in all samples. Blocky calcite cement, filling some of the dissolved foraminifera grains can be also seen. Rare dolomite crystals growing inside the foraminifera shells can be observed in some samples (Fig. 7b). Pyrite is relatively abundant. Pores are not connected and range in size from 0.02 to 0.5 mm.

(4) Laminated fine-grained organic-rich wackestone microfacies (FG OR WST): light grey–dark brown, organic-rich, poorly sorted, laminated microfacies type (Fig. 7e, f). Fish bone fragments, bivalve, benthic and planktonic foraminifera grains 15–140 μm in diameter are the dominant grain types. Organic matter is incorporated into the matrix filling microcracks and some parts of the foraminifera shells. The majority of foraminifera grains are cemented. According to EDS maps (Fig. 7f), the matrix is mainly calcareous. Visible porosity is of intraparticle type.

Major components, mineralogy and geochemistry

XRD analysis shows that carbonate (calcite and calcium magnesium carbonate) is the dominant mineral analysed in the study samples, with minor amounts of quartz, clay and apatite (Fig. 8). Pyrite and gypsum are locally abundant but, overall, are a minor fraction (<1% on average). This is consistent with many studies conducted on rock samples from the same interval (e.g. Khoury 2015; Alnawafleh *et al.* 2016; Gharaibeh 2017; Huggett *et al.* 2017; Sokol *et al.* 2017; Dhoun and Al-Zyod 2019; Ibrahim *et al.* 2019; Li *et al.* 2019).

Figure 9 shows average, minimum and maximum values of mineral fractions of all study microfacies types. JOS samples are particularly rich in carbonate, which constitutes more than 50% of the mineral content of three of the microfacies (OR MDST, OR WST and FG OR WST). Both OR WST and FG OR WST are primarily composed of carbonate, showing almost the same mean value (88 and 80%, respectively). OR MDST shows a lower average value of carbonate content (59%), while the carbonate mineral content is minor (35%) in SR PST.

Quartz is the second most abundant mineral, with the highest concentration in SR PST (up to 38%) compared to all the other microfacies. OR MDST has an average quartz value of 21% but shows a wide range (6–39%). Both OR WST and FG OR WST have the lowest quartz content of <4%.

Montmorillonite ($Al_2H_2O_{12}Si_4$) is the dominant clay mineral but, overall, has a low concentration and a relatively narrow range within all of the four identified microfacies types: OR MDST (7%), SR PST (11%), OR WST (5%) and FG OR WST (8%) (Fig. 9c).

Fish bone fragments are the major contributor to the apatite concentration, which has a mean value of around 7% (ranging from

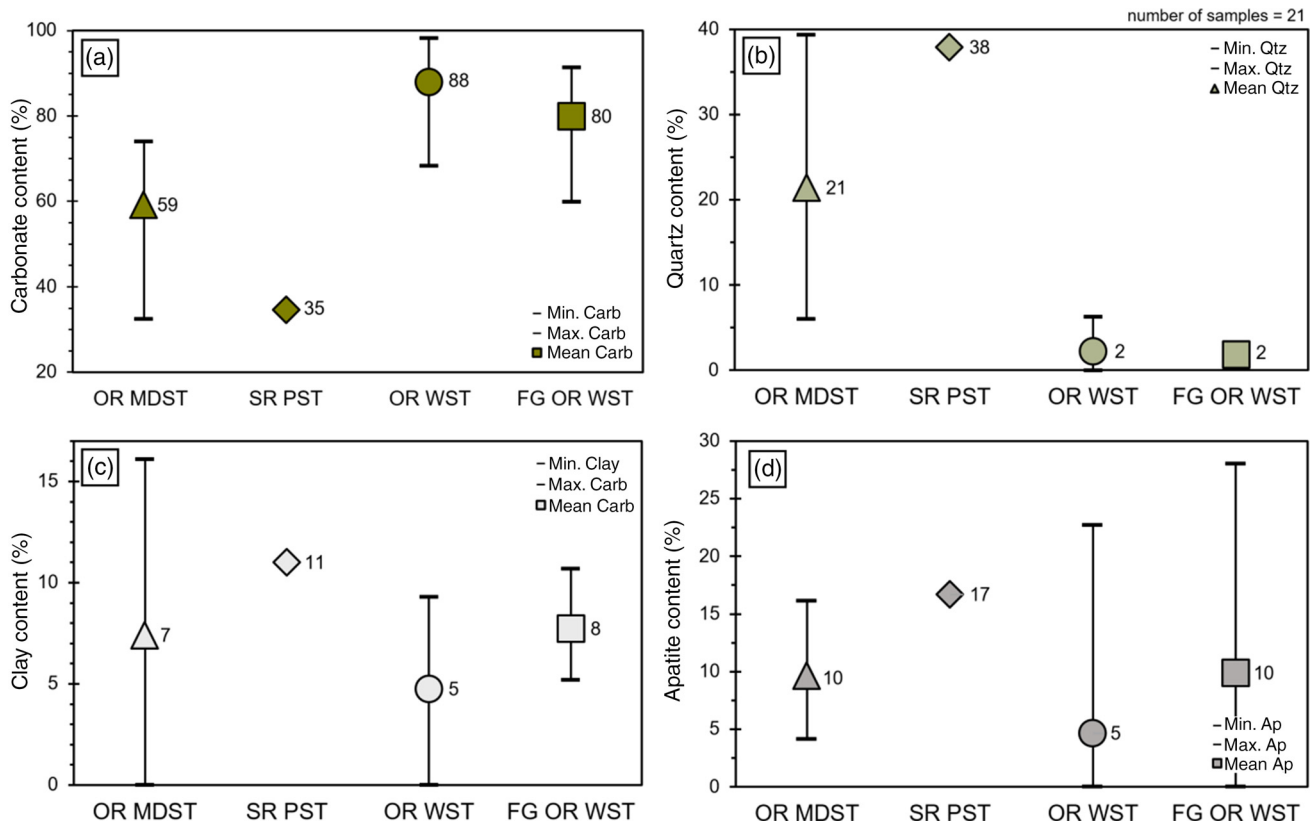

Fig. 9. Box plots demonstrating the distribution of (**a**) carbonate, (**b**) quartz, (**c**) clay and (**d**) apatite contents (average, minimum and maximum) among the four identified microfacies (21 samples tested). Note that OR WST and FG OR WST share similar properties in terms of carbonate and quartz content.

0 to 28%) in all of the samples. The highest apatite content belongs to SR PST.

Finally, the study samples have high TOC values that range from 8 to 25 wt% (Fig. 10). Peters and Cassa (1994) classified an excellent source rock as having TOC values exceeding 4 wt%. Here, even the silica-rich packstone microfacies type, which has the lowest TOC content of the four microfacies types, is considered excellent in terms of organic carbon richness, with values of 8 wt%. This richness in organic matter is attributed to a long period of regional high bioproductivity caused by the upwelling of nutrient-rich deep-marine waters that had encroached onto the shallow shelf (Abed 2013).

Rock mechanical and petrophysical characterization

Based on the scratch test results, OR MDST is observed to have the highest average UCS value, of 140 MPa, of the four identified microfacies (Fig. 11). SR PST has the second-highest average, with a value of 58 MPa, while OR WST and FG OR WST do not exceed 50 MPa. According to the ISRM classification (Clout and Manuel 2015), OR MDST and SR PST belong to the medium–high compressive strength intervals (50–250 MPa), while OR WST and FG OR WST can be classified as moderate (25–50 MPa).

The study samples exhibit a wide range of Leeb hardness (LH) values (Fig. 12), where SR PST is the hardest microfacies type

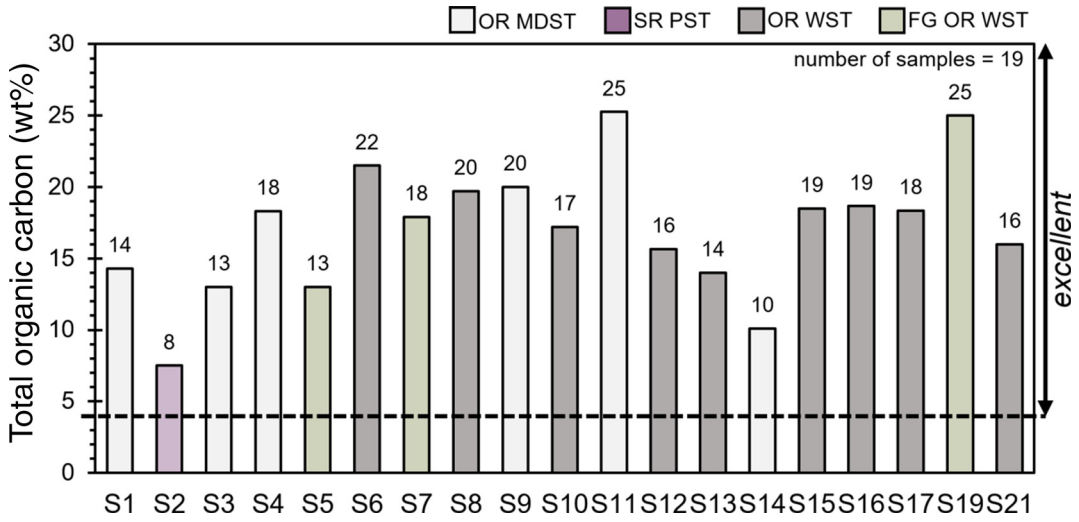

Fig. 10. Diagram showing the total organic carbon (TOC) content distribution within 19 tested samples. All samples belong to the upper 4–25 wt% interval, corresponding to excellent kerogen quality.

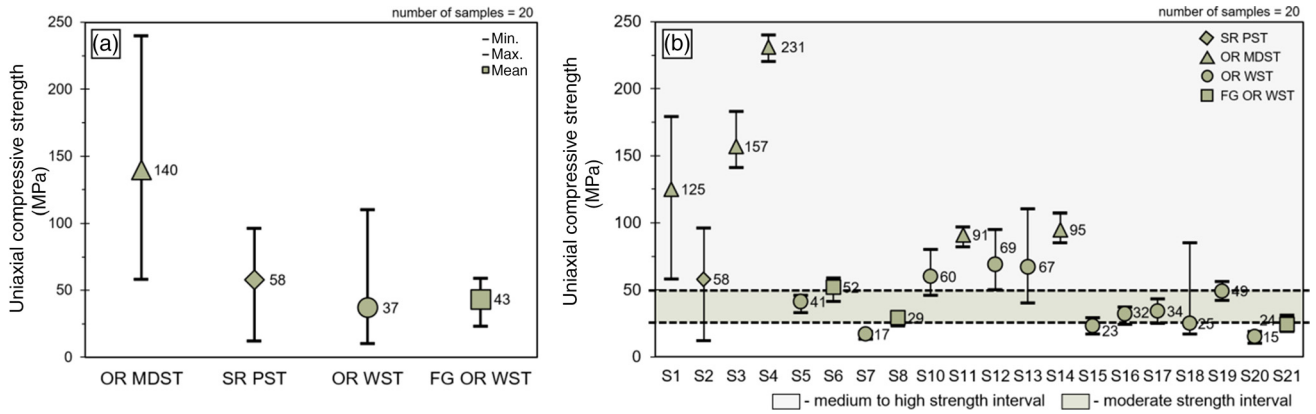

Fig. 11. Box plots of (**a**) uniaxial compressive strength values (mean, maximum and minimum) grouped by microfacies, revealing that the OR MDST microfacies type is the strongest; and (**b**) uniaxial compressive strength results for 20 samples.

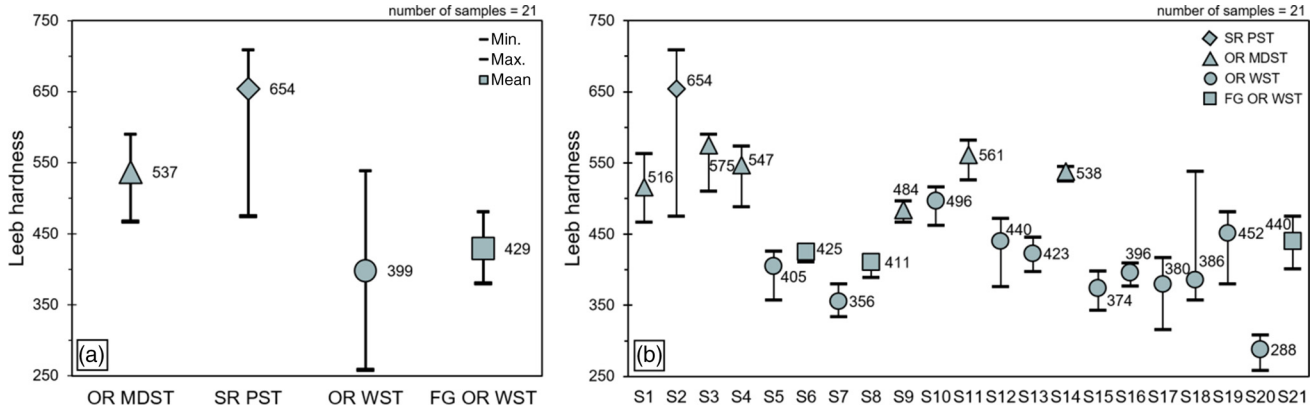

Fig. 12. Box plots displaying (**a**) Leeb hardness values (mean, maximum and minimum) grouped by microfacies; and and (**b**) Leeb hardness results for 21 tested Jordan oil shale samples.

(average of 654 LH), followed by OR MDST (average of 537 LH). However, OR WST and FG OR WST are softer. Their LH values are similar, at 399 and 429, respectively. The range of LH readings is relatively wide for SR PST and OR WST (234 and 280 LH unit range, respectively) compared to FG OR MDST (123 LH unit range) and FG OR WST (101 LH unit range), suggesting a more homogeneous texture of the latter compared to other microfacies.

The four microfacies subdivide into two groups (Fig. 13) based on their porosities. Both OR MDST and SR PST have low porosity values (≤6%), while OR WST and FG OR WST show high porosities (33 and 35%, respectively). The results obtained from the helium porosimetry correlate well with previously published porosity data (Terres *et al.* 2012). As we would expect, porosity values decrease with load and burial diagenesis.

OR MDST has the highest average compressional- and shear-wave velocities of 3368 and 1702 m s^{-1}, respectively (Fig. 14). OR WST and FG OR WST have lower average velocity readings. Owing to the specific sample dimension requirements needed for the sonic probe of the Epslog's Wombat scratch device, SR PST is not represented in the analysis.

Discussion

Elastic parameters and mineral composition

The types of minerals in the tested samples directly affect both the compressional- and shear-wave velocities. The quartz content has the most significant impact on the wave velocities (Fig. 15a). In the upper scatterplot of Figure 15b, two groups of samples can be distinguished: silica-rich samples (OR MDST), with the highest compressional-wave velocities; and carbonate-rich samples (OR WST and FG OR WST), with v_P values ranging between 1959 and 3368 m s^{-1}. The carbonate content correlates negatively with the compressional-wave velocities (correlation coefficients of 0.59: Fig. 15b). These results correlate well with the general finding of studies on similar types of rocks (e.g.

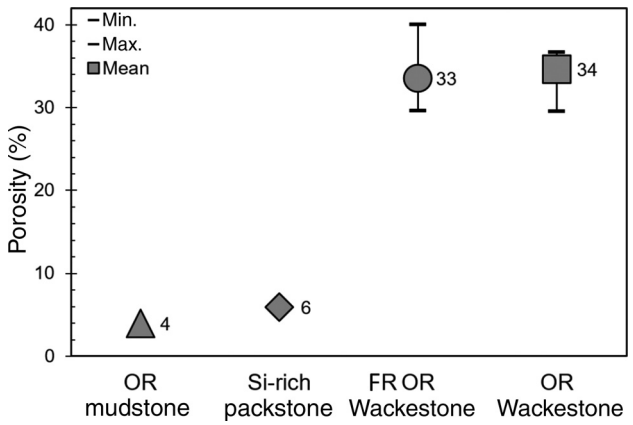

Fig. 13. Plot demonstrating porosity values (mean, maximum and minimum) grouped by microfacies. Note that samples can be clearly divided into two groups: low porous (OR mudstone and Si-rich packstone) and high porous (OR wackestone and FG OR wackestone).

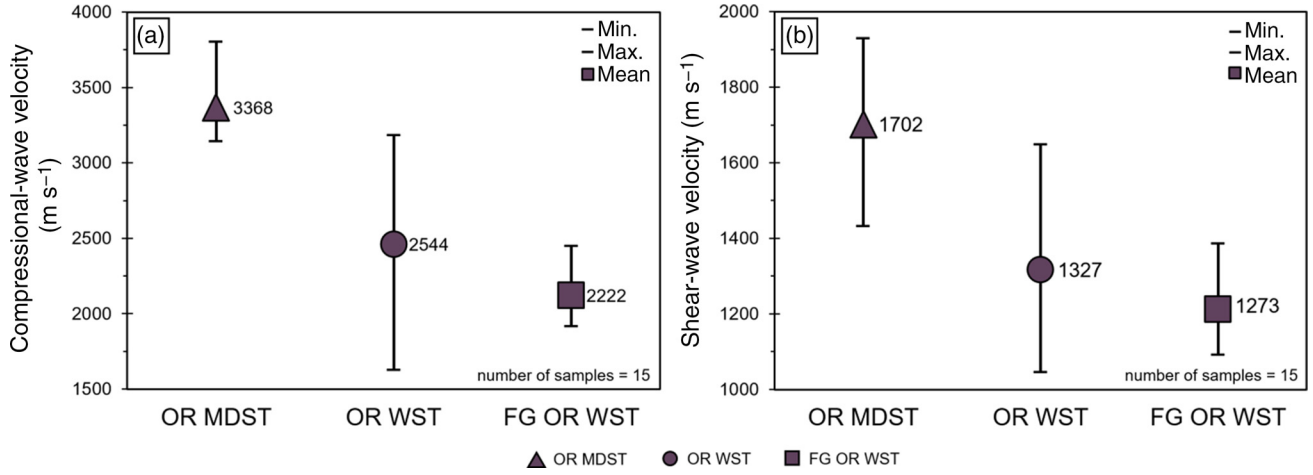

Fig. 14. Box plots presenting (**a**) compressional-wave and(**b**) shear-wave velocity values (mean, maximum and minimum) grouped by microfacies. Note that the OR MDST microfacies type has the highest average wave velocities. Owing to sample size requirements, SR PST is not represented here.

Vernik and Liu 1997; Quirein *et al.* 2012; Murphy *et al.* 2013). No correlation between the clay/TOC content and wave velocity was observed in this study.

Leeb hardness and mineral composition

Leeb hardness reflects the intrinsic properties of rocks, which are affected by the mineralogical composition, sample density, degree of cementation, rate of diagenesis, internal structure, type of matrix, presence of fractures and porosity (Koncagül and Santi 1999). Figure 16a–c presents scatterplots of the contents of the three frequently observed minerals (quartz (Fig. 16a), carbonate (Fig. 16b) and clay (Fig. 16c)) against LH measurement, while Figure 16d shows the TOC content against LH measurement. The abundance of the authigenic quartz (biogenic silica) content is a major factor affecting the Leeb hardness results, which is reflected by the positive correlation between them (Fig. 16a). Figure 16e demonstrates an example of the heterogeneity of the sample affected by the presence of a silica-filled fracture, which increases the

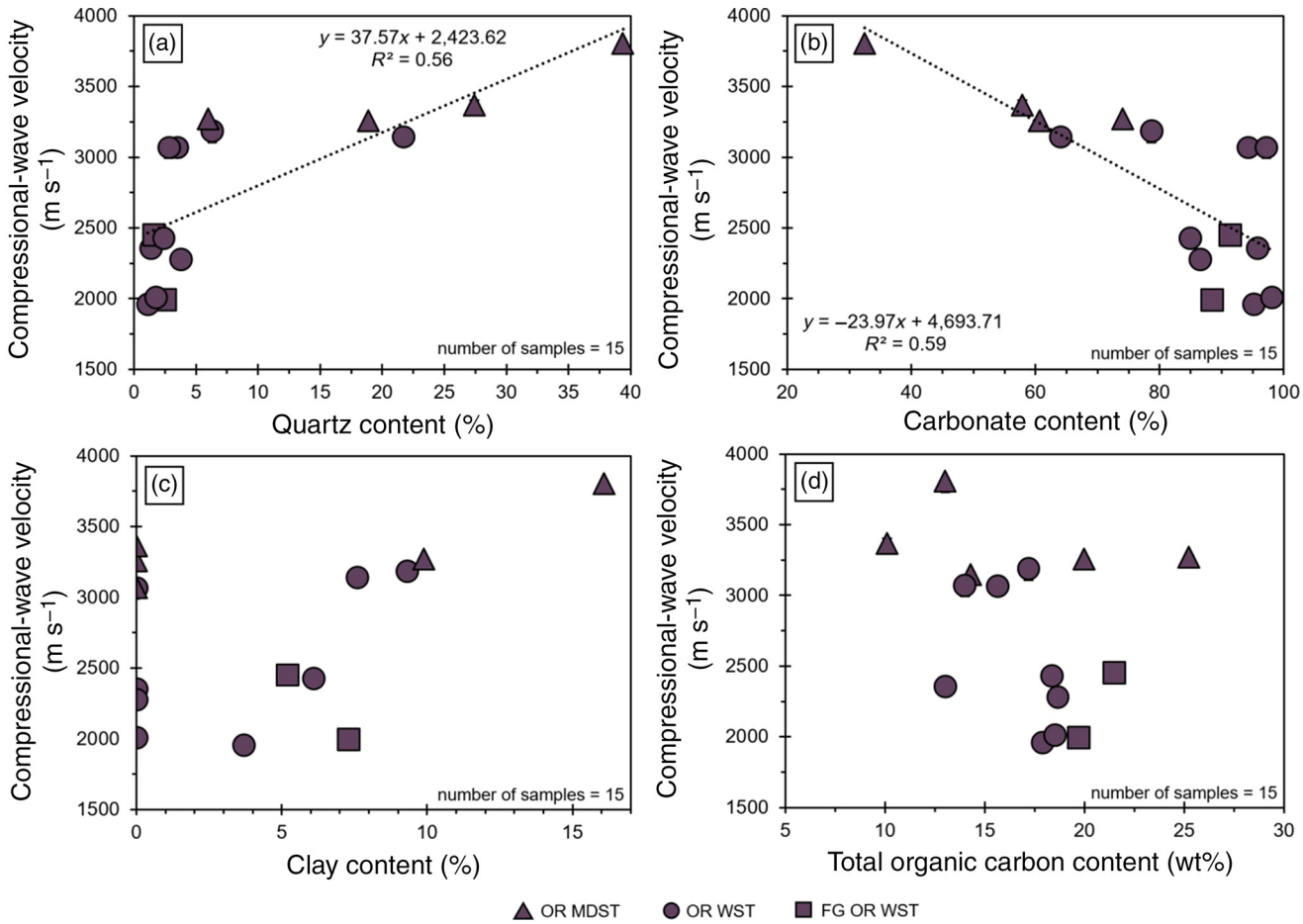

Fig. 15. Relationship between compressional-wave velocities and (**a**) quartz, (**b**) carbonate, (**c**) clay and (**d**) total organic carbon (TOC) content. No clear trend can be observed between the clay/TOC content and compressional-wave velocities.

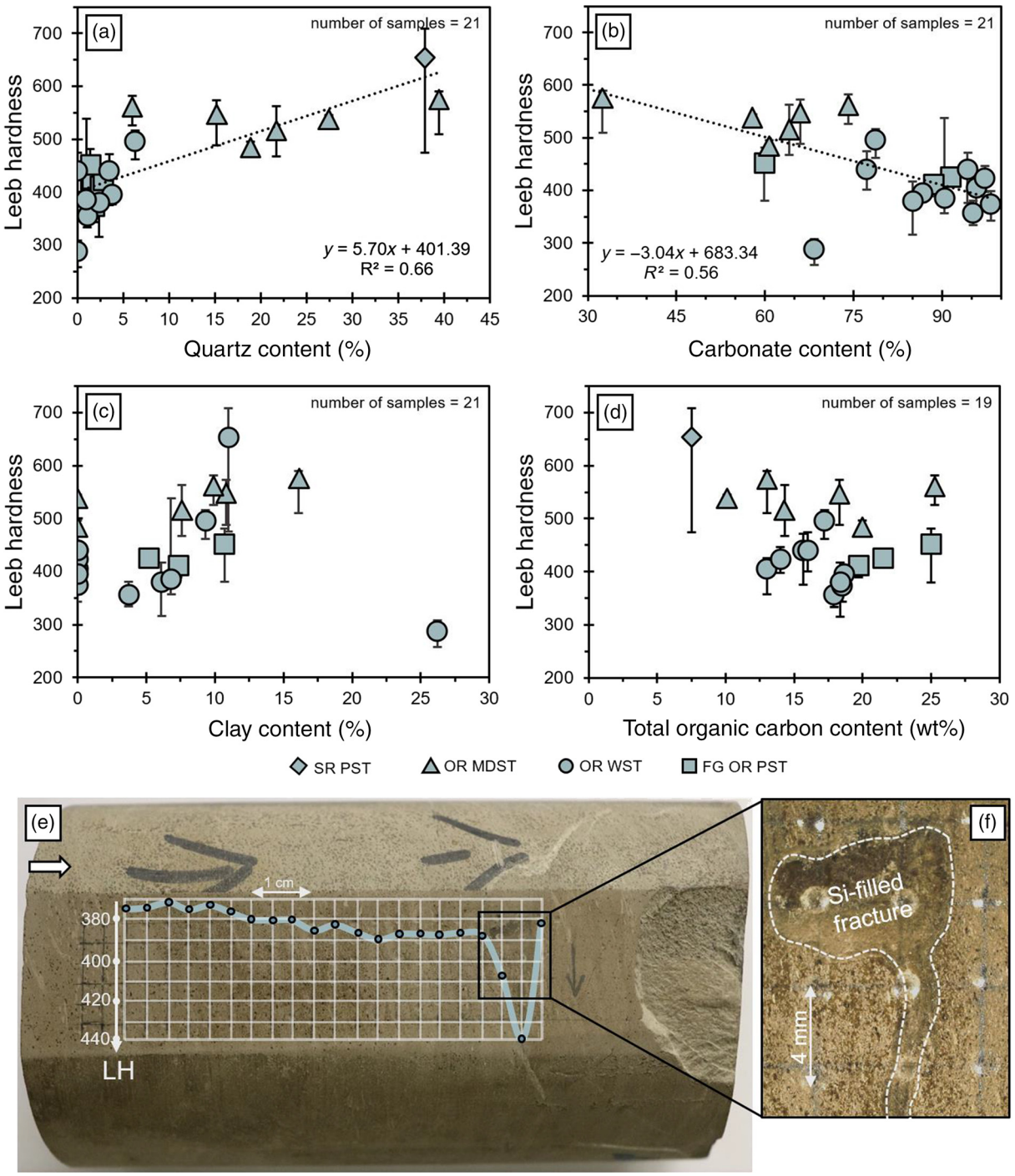

Fig. 16. Relationship between (**a**) quartz, (**b**) carbonate, (**c**), clay and (**d**) total organic carbon (TOC) and Leeb hardness measurements. (**e**) Demonstrating an increase in Leeb hardness (LH) values with the presence of a silica-filled fracture. Inset (**f**) showing a silica-filled fracture after Leeb hardness testing.

hardness of the sample by 15%. In addition, the carbonate concentration shows a negative correlation with LH, indicating low hardness values for samples that include a carbonate fraction higher than that of quartz (Fig. 16b). This compares very well with observations from several studies where certain minerals (e.g. quartz) provide stronger bonding than other types of minerals (e.g. calcite or clay) (Vutukuri *et al.* 1974; Dong *et al.* 2017). Clay concentrations show no clear correlation with LH, indicating no significant effect of clay on LH. This is related to the relatively small concentrations of clay in the samples compared to quartz and calcite in this study (Fig. 16c). The TOC shows a slight negative correlation with LH, indicating that the rock hardness decreases with an increase in TOC.

The quartz was originally a metastable biogenic opaline alpha silica that originated from radiolarian and diatom shells (Huggett *et al.* 2017). The EDS maps suggest that this quartz was recrystallized/stabilized apparently into a siliceous matrix frame. The LH correlation with clay and TOC is a co-correlation between these components and the quartz content. This is well corroborated by Figure 16e, which shows an increased hardness over the silica-filled fracture.

Figure 17 shows that SR PST and OR MDST fall in the LH range of 500–750, whereas OR WST and FG OR WST show lower LH values in the range of 250–500. The threshold of *c.* 500 LH can be used to effectively differentiate between microfacies with a high quartz content (OR MDST and SR PST) and quartz-poor

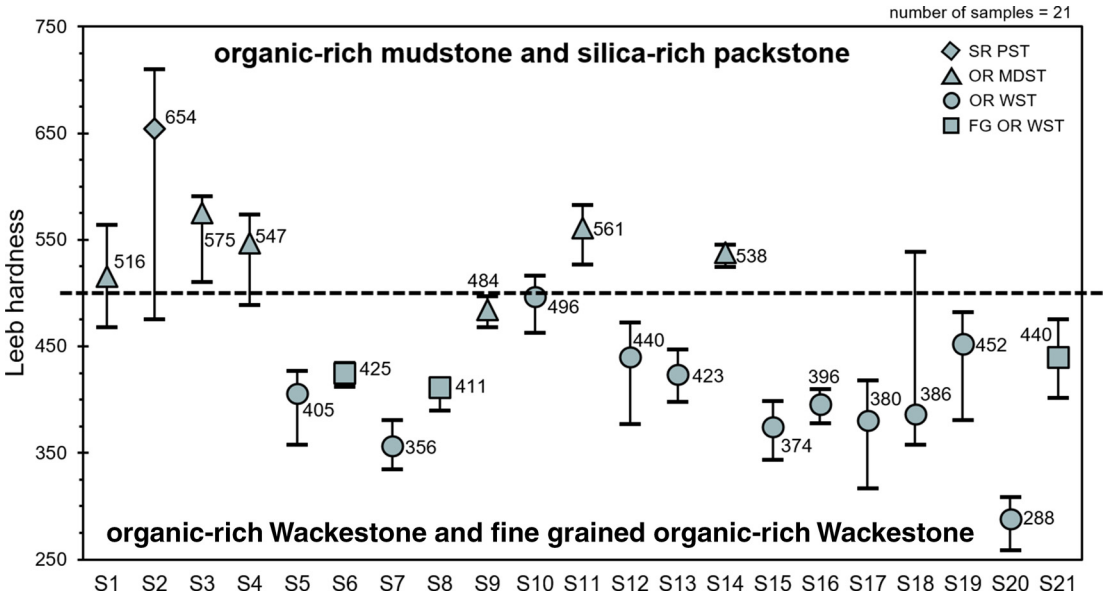

Fig. 17. Leeb hardness results showing that OR MDST and SR PST fall in the upper range Leeb hardness values of 500–750, while OR WST and FG OR WST belong to the lower 250–500 range.

microfacies (OR WST and FG OR WST). As the silica in the studied samples is biogenic, it might reflect some differences/shifts in the oceanographic system between silica-rich and silica-poor settings based on where in the basin the sample was collected or could be also attributed to the changes in primary biogenic productivity over time (cyclicity).

Uniaxial compressive strength and mineral composition

The UCS values depend on several parameters, such as rock type, rock composition, rock grain size, rock density and porosity, rock anisotropy, water pore pressure and saturation, and temperature (Golodkovskaia *et al.* 1975; Meehan *et al.* 1975; Tarrer and Wagh 1991; Irfan 1996; Agustawijaya 2007). In the present study, UCS was derived using a scratch device (Epslog Wombat).

Figure 18 illustrates the influence of the three frequently observed minerals (quartz, carbonate and clay) and the TOC content on the UCS. Based on the results, only the quartz concentration is moderately correlated with UCS, with a correlation coefficient of 0.36 (Fig. 18a). Other minerals, such as clay and carbonate, reveal a weak but noticeable negative correlation (0.26 for carbonate) or no correlation. With increasing clay content, OR MDST and OR WST show higher UCS values.

In addition, calcium-rich laminations significantly decrease UCS values compared to samples of a siliceous matrix (Fig. 18e). The TOC content shows no correlation with the UCS readings. Thus, mineralogy is not considered a significant factor controlling the intrinsic specific energy (the energy required to cut a unit volume of rock, which reflects the strength of the rock). The effective porosity correlates well with the rock strength, suggesting that porosity plays a key role in controlling the rock strength. The same trend was documented by several researchers, showing that high porosity values of rocks are expected to exhibit low strength (Al-Harthi *et al.* 1999; Li and Wang 2019).

Brittle–ductile behaviour evaluation

There is no unique universally accepted rock brittleness definition (Ye *et al.* 2020). Instead, different researchers use the term 'brittleness' differently. It can be defined as a lack of ductility (Hetenyi 1950), the capability of rocks to self-sustain fracturing (Tarasov and Potvin 2013), the destruction of internal cohesion (Ramsey 1967) or the ability of a formation to deform with a low degree of inelastic behaviour (Andreev 1995). However, the brittleness index (BI) in most studies is known as a key parameter in the planning of successful hydraulic fracturing, especially in unconventional reservoirs with low porosity (<10%) and ultra-low permeability (<0.1 mD) (Zou *et al.* 2012; Gensterblum *et al.* 2015; Aguilera 2016; Mews *et al.* 2019). Brittle rock formations are more likely to become fractured and respond better to hydraulic fracturing than ductile layers. Thus, a good understanding of the BI is necessary to identify favourable zones for hydrofracturing (Ariketi *et al.* 2017). The BI helps in evaluating whether a rock formation can easily form complex fracture networks, which in turn increases production if the fracture networks are interconnected (Grieser and Bray 2007).

As the TOC values in the JOS are extremely high (Fig. 10), the BI was estimated based on the mineralogy proposed by Wang and Gale (2009), $BI_{W\&G}$, but we also included TOC as a parameter as TOC values are extremely high in the JOS:

$$BI_{W\&G} = \frac{Qz + Dol}{Qz + Ca + Clay + Dol + TOC} \quad (4)$$

where Qz is the quartz content, Dol is the dolomite content, Ca is the calcite content, Clay is the clay content and TOC is the total organic carbon by fraction in the rock. Figure 19 shows high BI values for both OR MDST and SR PST. Hence, they can be classified as brittle rocks, with the brittleness derived from their siliceous matrix (see Figs 6b and 9b) and lower TOC content (in the case of the SR PST). In contrast, OR WST and FG OR WST can be categorized as highly ductile. Low BI values for both OR WST and FG OR WST are related to the high average carbonate concentration (88 and 80%, respectively), implying a ductile material.

Furthermore, these microfacies contain the lowest content of quartz (<5%), which is considered to be the major mineral contributing to the brittleness of the rocks. The relatively high brittleness ranges in OR MDST and SR PST are explained by the large variability of the quartz content in these samples. Silica diagenesis may have played an important role in the increasing brittleness values. The recrystallization of the biogenic opaline silica into a quartz matrix may also lead to an increase in brittleness.

The mineral-derived BI correlates well with measured LH readings, showing a correlation coefficient of 0.72 (Fig. 20a).

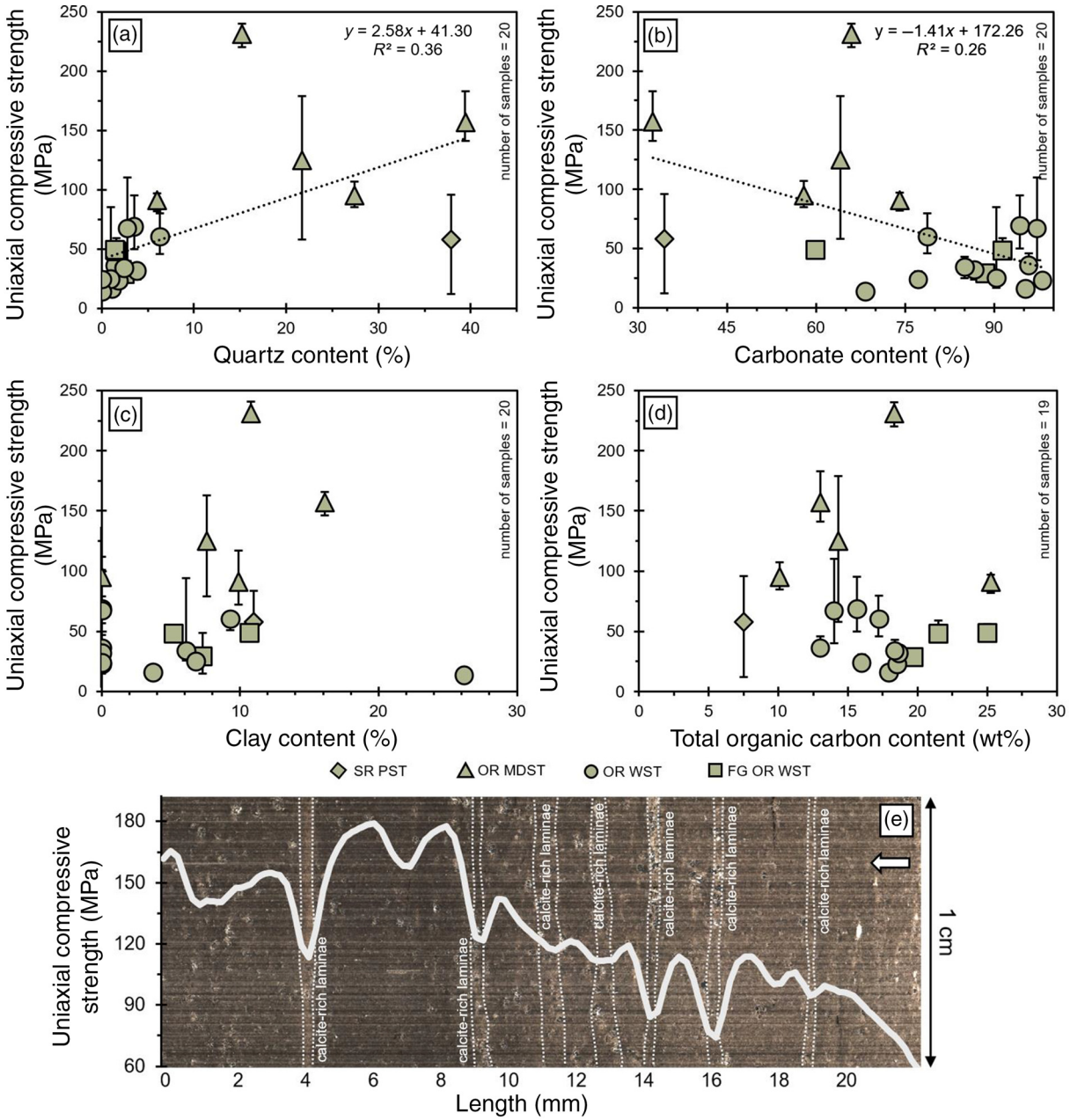

Fig. 18. Relationship between (**a**) quartz, (**b**) carbonate, (**c**) clay and (**d**) TOC and uniaxial compressive strength measurements. (**e**) Demonstrating a decrease in uniaxial compressive strength values for calcite-rich lamina (highlighted in dotted lines) and an overall trend with an increased occurrence of calcite-rich laminations to the right. Note the decline in uniaxial compressive strength values with the change in the rock colour (from dark on the left to light on the right), indicating a strong relationship with rock composition.

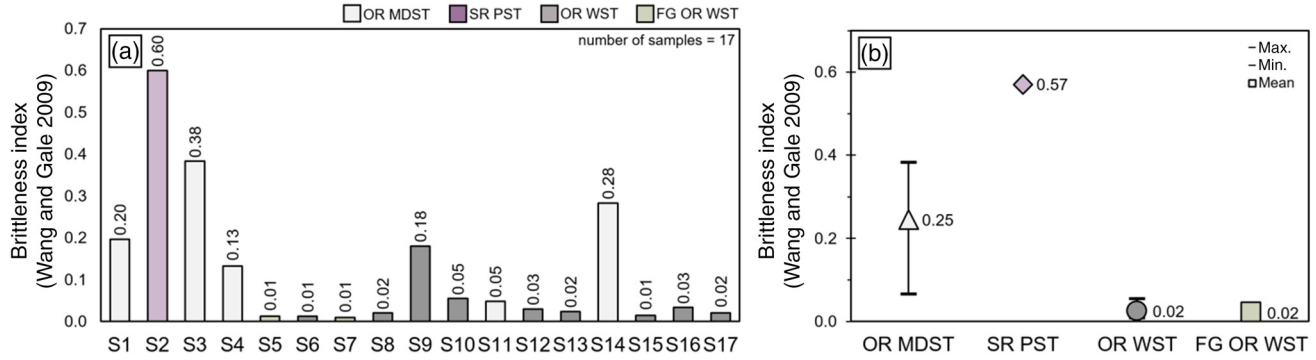

Fig. 19. (**a**) Brittleness index values for 17 studied samples. (**b**) Brittleness index values (mean, minimum and maximum) for the four identified types of microfacies.

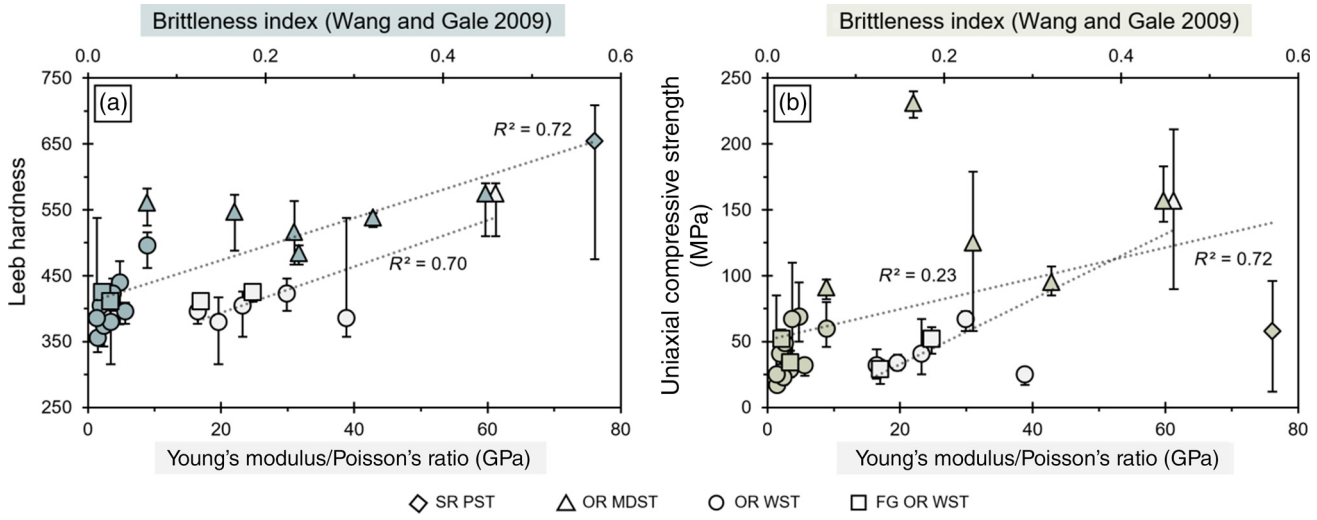

Fig. 20. (**a**) Leeb hardness v. mineral-derived brittleness index (blue) and Young's modulus/Poisson's ratio (light grey). (**b**) Uniaxial compressive strength v. mineral-derived brittleness index (green) and Young's modulus/Poisson's ratio (light grey).

UCS shows a similar overall trend of increased values with an increased mineral-derived BI (Fig. 20b). However, SR PST does not follow the trend line, which can be explained by the highly heterogeneous nature of the microfacies whose increased number of laminations (compared to other microfacies types) consist of large cemented grains (mainly fish bone fragments) (see Fig. 6a). This indicates that the fabric may impact LH readings more than the brittle mineral concentration.

The elastic-based BI depends on both the Poisson's ratio, which can help to characterize the transverse deformation intensity of rocks (Pan *et al.* 2020), and Young's modulus, which indicates the stiffness of the formation (Mews *et al.* 2019). One of the definitions that predominant in the geophysical literature states that rocks with a high brittle index values have a high Young's modulus and a low Poisson's ratio. In comparison, rocks with large Poisson's ratio and low Young's modulus tend to have a low BI and are usually ductile (Grieser and Bray 2007; Rickman *et al.* 2008; Goodway *et al.* 2010; Sharma and Chopra 2012; Luan *et al.* 2014; Herwanger *et al.* 2015). Formations with high Young's modulus and low Poisson's ratio will experience brittle failure along their shear planes, as the shear modulus tends to be higher under such conditions (Jahandideh and Jafarpour 2016). These rocks experience fewer axial and radial strains under the same force applied. Thus, rocks with these properties can convert absorbed energy into elastic energy to promote the initiation and creation of cracks (Ye *et al.* 2020).

Although our approach does not calculate the value of the BI, it can help to evaluate qualitatively the relative ductile/brittle behaviour of rocks and confirm the results of mineral-derived BI. The lower *x*-axis in Figure 20a and b represents values of Young's modulus divided by Poisson's ratio (light blue in Fig. 20a and light grey in Fig. 20b) for selected samples, suggesting higher values for brittle samples (as discussed before). Strong positive correlations were observed between both the measured LH and YM/PR ratio, and UCS and YM/PR ratio, yielding correlation coefficients of 0.7 and 0.72, respectively (Fig. 20a, b). The good correlation coefficient between LH and mineral-derived BI, LH and YM/PR, and UCS and YM/PR suggests that LH and UCS measurements are useful proxies for BI evaluation. Moreover, LH readings can be used as a quick and accurate criterion for brittleness.

Overall, the results of the material stiffness correspond with the rock strength, indicating that the OR MDST microfacies is stiff (20 GPa) and strong (140 MPa), followed by OR WST and FG OR WST, which are less stiff (7.3 and 5.4 GPa, respectively) and less strong (37 and 43 MPa, respectively).

Implications

The findings of this research are significant in the way in which they can be used for more efficient exploitation of the JOS. A good understanding of the vertical and regional distribution of microfacies will allow an estimation of the rock mechanical properties (e.g. brittleness index) and the selection of favourable areas for surface mining operations. The quantification of elastic v. plastic (or non-elastic) and brittle v. ductile behaviour has an important implication for reservoir stimulation success not only with respect to rock mechanical behaviour but also for the least principal stress variability (Sone and Zoback 2013, 2014). The unique nature of the Jordan source rocks (i.e. organic-rich and immature) make them an analogue for unconventional source-rock plays that are of similar origin and composition (e.g. the Shilaif Formation in the United Arab Emirates, Najmah shales in Kuwait, and Tuwaiq Mountain and the Hanifa Formation in Saudi Arabia). These source rocks, with their relatively similar mineralogical composition and depositional settings, may behave or exhibit a relationship between microfacies and rock mechanical properties similar to the results established here for the Jordan source rocks. Rock mechanical properties in these unconventional reservoirs could be predicted in uncored wells using petrophysical logs if such a correlation can be established between microfacies and properties, keeping in mind the diagenesis that these rocks experienced during maturation. This may aid cost-efficient exploitation by significantly saving the costs of identifying artificial stimulation intervals.

Conclusion

The compositionally diverse Upper Cretaceous Jordanian organic-rich carbonate mudrocks provide insights into the change of rock mechanical properties within different lithofacies. Based on the performed petrophysical, geochemical and rock mechanical tests, supported by optical microscopy observations, the results of this study revealed that:

(1) The Jordanian organic-rich carbonate mudrock samples are lithologically heterogeneous and represent four microfacies, according to Dunham's (1962) classification, including organic-rich mudstone, silica-rich packstone, organic-rich wackestone and fine-grained organic-rich wackestone.
(2) Leeb hardness test results are affected by the mineral composition of the sample. A high quartz content was shown to increase the Leeb hardness values, whereas an

increase in the carbonate content led to a reduction of Leeb hardness values. The scratch-derived uniaxial compressive strength (UCS) readings are affected by both the mineral composition and the porosity. Quartz tends to increase the UCS, while carbonate material leads to a reduction in the UCS.

(3) The data show no correlation between the scratch-derived UCS and the total organic carbon (TOC) content, or between wave velocity and the TOC, and it has minimal effect on the Leeb hardness readings.

(4) The mineral-based brittleness index (BI) and the qualitative elastic-properties-based approach show similar results, suggesting that organic-rich mudstone and silica-rich packstone microfacies are more brittle compared to organic-rich wackestone and fine-grained organic-rich wackestone.

(5) A good correlation coefficient between Leeb hardness and the mineral-derived BI (0.72), the Leeb hardness and Young's modulus/Poisson's ratio (0.7), and the UCS and Young's modulus/Poisson's ratio (0.72) suggests that Leeb hardness and UCS measurements are useful proxies for the BI evaluation. Leeb hardness readings can be used as a quick and accurate criterion for brittleness estimation.

Acknowledgements The authors extend their gratitude to the Ministry of Energy and Mineral Resources of Jordan (MEMR) for providing the core samples used in this study from cored wells drilled by Royal Dutch Shell through the unique immature carbonate source rocks of Jordan. The authors are grateful to the editor and reviewers (John Powell and the anonymous reviewer) for the positive feedback and their insightful and helpful comments.

Author contributions **ISA**: conceptualization (lead), data curation (lead), formal analysis (equal), funding acquisition (supporting), investigation (lead), methodology (lead), project administration (lead), resources (lead), software (equal), supervision (lead), validation (lead), visualization (lead), writing – original draft (lead), writing – review & editing (lead); **RI**: conceptualization (equal), data curation (equal), formal analysis (lead), investigation (equal), methodology (equal), project administration (equal), software (supporting), validation (equal), visualization (equal), writing – original draft (equal), writing – review & editing (equal); **TF**: formal analysis (supporting), investigation (supporting), methodology (supporting), project administration (supporting), resources (supporting), supervision (supporting), validation (equal), writing – review & editing (supporting); **JC**: investigation (supporting), methodology (supporting), supervision (supporting), validation (equal), writing – review & editing (supporting); **VV**: conceptualization (supporting), data curation (supporting), formal analysis (supporting), funding acquisition (lead), investigation (supporting), methodology (supporting), project administration (equal), resources (supporting), supervision (lead), validation (supporting), writing – original draft (supporting), writing – review & editing (supporting).

Funding This work was funded by the King Abdullah University of Science and Technology (KAUST) (grant number 1399-01-01).

Competing interests The authors declare that they have no known competing financial interests or personal relationships that could have appeared to influence the work reported in this paper.

Data availability All data generated or analysed during this study are included in this published article (and its supplementary information files). The raw data used in this article are available from the corresponding author.

References

Abed, A.M. 2013. The eastern Mediterranean phosphorite giants: an interplay between tectonics and upwelling. *GeoArabia*, **18**, 67–94, https://doi.org/10.2113/geoarabia180267

Abed, A.M. and Amireh, B.S. 1983. Petrography and geochemistry of some Jordanian oil shales from North Jordan. *Journal of Petroleum Geology*, **5**, 261–274, https://doi.org/10.1111/j.1747-5457.1983.tb00571.x

Abed, A.M., Arouri, K.H. and Boreham, C.J. 2005. Source rock potential of the phosphorite bituminous chalk–marl sequence in Jordan. *Marine and Petroleum Geology*, **22**, 413–425, https://doi.org/10.1016/j.marpetgeo.2004.12.004

Abu-Hamatteh, Z., Jaber, J., Besieso, M., Al-Jufout, S., Al-Azab, T. and Al-Shawabkeh, A. 2008. Jordanian oil shale: a promising strategic source of energy. *In*: White, J.R. and Robinson, W.H. (eds) *Natural Resources, Economics, Management and Policy*. Nova Science, New York, 89–129.

Abu-Mahfouz, I.S., Cartwright, J., Idiz, E., Hooker, J., Robinson, S. and Boorn, S. 2019. Genesis and role of bitumen in fracture development during early catagenesis. *Petroleum Geoscience*, **25**, 371–388, https://doi.org/10.1144/petgeo2018-179

Abu-Mahfouz, I.S., Cartwright, J., Idiz, E., Hooker, J.N. and Robinson, S. 2020*a*. Silica diagenesis promotes early primary hydrocarbon migration. *Geology*, **48**, 483–487, https://doi.org/10.1130/G47023.1

Abu-Mahfouz, I.S., Cartwright, J., Vahrenkamp, V., Patzek, T. and Littke, R. 2020*b*. Fracture development in unconventional reservoirs & its role in hydrocarbon migration & expulsion. AAPG Search and Discovery paper, AAPG Annual Convention and Exhibition (ACE) 2020, 7–10 June 2020, virtual meeting.

Abu-Mahfouz, I.S., Gaus, G. *et al.* 2022*a*. Improved understanding of hydrocarbon expulsion and associated fracturing during successive stages of maturation: Insights from the artificial maturation of organic-rich, immature to early mature source rocks. Paper IPTC-21895-MS presented at the International Petroleum Technology Conference and Exhibition (IPTC 2022), 21–23 February 2022, Riyadh, Saudi Arabia, https://doi.org/10.2523/IPTC-21895-MS

Abu-Mahfouz, I.S., Wicaksono, A.N., Idiz, E., Cartwright, J., Santamarina, J.C. and Vahrenkamp, V.C. 2022*b*. Modelling the initiation of bitumen-filled microfractures in immature, organic-rich carbonate mudrocks: The Maastrichtian source rocks of Jordan. *Marine and Petroleum Geology*, **141**, 105700, https://doi.org/10.1016/j.marpetgeo.2022.105700

Aguilera, R. 2016. Shale gas reservoirs: Theoretical, practical and research issues. *Petroleum Research*, **1**, 10–26, https://doi.org/10.1016/S2096-2495(17)30027-3

Agustawijaya, D.S. 2007. The uniaxial compressive strength of soft rocks. *Civil Engineering Dimension*, **9**, 9–14, http://puslit.petra.ac.id/journals/civil

Ajalloeian, R., Mansouri, H. and Baradaram, E. 2017. Some carbonate rock texture effects on mechanical behavior, based on Koohrang tunnel data, Iran. *Bulletin of Engineering Geology and the Environment*, **76**, 295–307, https://doi.org/10.1007/s10064-016-0861-y

Alali, J. 2006. Jordan Oil Shale, availability, distribution, and investment opportunity. Paper rtos-A117 presented at the International Conference on Oils Shale: 'Recent Trends in Oil Shale', 7–9 November 2006, Amman, Jordan.

Al-Harthi, A.A., Al-Amri, R.M. and Shehata, W.M. 1999. The porosity and engineering properties of vesicular basalt in Saudi Arabia. *Engineering Geology*, **54**, 313–220, https://doi.org/10.1016/S0013-7952(99)00050-2

Ali Hussein, M., Alqudah, M., van den Boorn, S., Kolonic, S., Podlaha, O.G. and Mutterlose, J. 2014. Eocene oil shales from Jordan – their petrography, carbon and oxygen stable isotopes. *GeoArabia*, **19**, 139–162, https://doi.org/10.2113/geoarabia1903139

Ali Hussein, M., Alqudah, M., Blessenohl, M., Podlaha, O. and Mutterlose, J. 2015. Depositional environment of Late Cretaceous to Eocene organic-rich marls from Jordan. *GeoArabia*, **20**, 191–210, https://doi.org/10.2113/geoarabia2001191

Almogi-Labin, A., Bein, A. and Sass, A. 1993. Late cretaceous upwelling system along the southern Tethys margin (Israel): interrelationship between productivity, bottom water environments, and organic matter preservation. *Paleoceanography*, **8**, 671–690, https://doi.org/10.1029/93PA02197

Alnawafleh, H., Tarawneh, K., Siavalas, G., Christanis, K. and Iordanidis, A. 2016. Geochemistry and organic petrography of Jordanian Sultani Oil Shale. *Open Journal of Geology*, **6**, 1209–1220, https://doi.org/10.4236/ojg.2016.610089

Alqudah, M., Hussein, M.A., Podlaha, O.G., Boorn, S., Kolonic, S. and Mutterlose, J. 2014. Calcareous nanofossil biostratigraphy of Eocene oil shales from central Jordan. *GeoArabia*, **19**, 117–140, https://doi.org/10.2113/geoarabia1901117

Alqudah, M., Hussein, M.A., van den Boorn, S., Podlaha, O.G. and Mutterlose, J. 2015. Biostratigraphy and depositional setting of Maastrichtian–Eocene oil shales from Jordan. *Marine and Petroleum Geology*, **60**, 87–104, https://doi.org/10.1016/j.marpetgeo.2014.07.025

Amireh, B.S. 1996. Sedimentology and paleogeography of the regressive–transgressive Kurnub Group (Early Cretaceous) of Jordan. *Sedimentary Geology*, **112**, 69–88, https://doi.org/10.1016/S0037-0738(97)00024-9

Andreev, G.E. 1995. *Brittle Failure of Rock Materials*. A.A. Balkema, Rotterdam, The Netherlands.

Ariketi, R., Bhui, U.K., Chandra, S. and Biswal, S. 2017. Brittleness modeling of Cambay shale formation for shale gas exploration: a study from Ankleshwar area, Cambay Basin, India. *Journal of Petroleum Exploration and Production Technology*, **7**, 911–923, https://doi.org/10.1007/s13202-017-0326-2

ASTM 2001. *Standard Test Method for Determination of Rock Hardness by Rebound Hammer Method*. ASTM Standard 04.09 (D 5873-00). American Society for Testing and Materials (ASTM), West Conshohocken, PA.

Baaske, P. 2005. *Sequence Stratigraphy, Sedimentology and Provenance of the Upper Cretaceous Siliciclastic Sediments of South Jordan*. Doctoral thesis, University of Stuttgart, Stuttgart, Germany.

Bandel, K. and Salameh, E.M. 2013. *Geologic Development of Jordan: Evolution of its Rocks and Life*. University of Jordan, Amman.
Bender, F.K. 1968. *Geologie von Jordanien*. Beitrage zur Regionalen Geologie der Erde, **7**. Gebruder Borntraeger, Berlin.
Brunhoeber, O.M., Arakkal, D., Ji, R., Miletić, M. and Beckingham, L.E. 2020. Impact of mineral composition and distribution on the mechanical properties of porous media. *E3S Web of Conferences*, **205**, 02006, https://doi.org/10.1051/e3sconf/202020502006
Burdon, D.J. 1959. *Handbook of Geology of Jordan: To Accompany and Explain Three Sheets of the 1:250 000 Geological Map of Jordan East of the Rift by A.M. Quennell*. Government of the Hashemite Kingdom, Amman.
Butterlin, J., Vrielynck, B. *et al.* 1993. Lutetian, (46–40 Ma). *In*: Dercourt, J., Ricou, L. and Vrirlynck, B. (eds) *Atlas of Tethys Paleoenvironmental Maps*. Beicip-Franlab, Rueil-Malmaison, France, 197–209.
Clout, J.M.F. and Manuel, J.R. 2015. Mineralogical, chemical, and physical characteristics of iron ore. *In*: Lu, L. (ed.) *Iron Ore: Mineralogy, Processing and Environmental Sustainability*. Woodhead Publishing, Cambridge, UK, 45–84, https://doi.org/10.1016/B978-1-78242-156-6.00002-2
Dagrain, F., Poyol, E. and Richard, T. 2004. Strength logging of geomaterials from scratch tests. *In*: Schubert, W. (ed.) *Rock Engineering – Theory and Practice: Proceedings of the ISRM Regional Symposium EUROCK 2004 & 53rd Geomechanics Colloquy*. Glückauf, Essen, Germany, 635–640.
Day, M. 1977. Field assessment of rock hardness using the Schmidt test hammer. *British Geomorphological Research Group Technical Bulletin*, **18**, 19–29.
Dhoun, H. and Al-Zyod, S. 2019. Geochemical assessments and potential energy sources evaluations based on oil shale and geothermal resource in Wadi Al-Shallala–North Jordan. *International Journal of Geosciences*, **10**, 351–365, https://doi.org/10.4236/ijg.2019.103020
Diabat, A. and Masri, A. 2005. Orientation of the principal stresses along Zerqa-Ma'in Fault. *Mu'tah Lil-Buhuth wad-Dirasat*, **20**, 57–71.
Dong, T., Harris, N.B., Ayranci, K. and Yang, S. 2017. The impact of rock composition on geomechanical properties of a shale formation: middle and Upper Devonian Horn River Group shale, Northeast British Columbia, Canada. *AAPG Bulletin*, **101**, 177–204, https://doi.org/10.1306/07251615199
Dunham, R.J. 1962. Classification of carbonate rocks according to depositional texture. *In*: Ham, W.E. (ed.) *Classification of Carbonate Rocks*. AAPG, Tulsa, OK, 108–121.
Dyni, J.R. 2006. *Geology and Resources of Some World Oil-Shale Deposits*. United States Geological Survey Scientific Investigations Report 2005-5294.
Eberli, G.P., Baechle, G., Anselmetti, F.S. and Incze, M.L. 2003. Factors controlling elastic properties in carbonate sediments and rocks. *The Leading Edge*, **22**, 654–660, https://doi.org/10.1190/1.1599691
Fjær, E., Holt, R.M., Horsrud, P., Raaen, A.M. and Risnes, R. 2008. Geological aspects of petroleum related rock mechanics. *In*: Fjær, E., Holt, R.M., Horsrud, P., Raaen, A.M. and Risnes, R. (eds) *Petroleum Related Rock Mechanics*. 2nd edn. Developments in Petroleum Science, **53**. Elsevier, Amsterdam, 103–133, https://doi.org/10.1016/S0376-7361(07)53003-7
Gensterblum, Y., Ghanizadeh, A. *et al.* 2015. Gas transport and storage capacity in shale gas reservoirs – A review. Part A: Transport processes. *Journal of Unconventional Oil and Gas Resources*, **12**, 87–122, https://doi.org/10.1016/j.juogr.2015.08.001
Germay, C. and Richard, T. 2014. The scratch test: a high-resolution log of rock strength with application to geomechanics and petrophysics. Paper SPWLA-2014-WW presented at the SPWLA 55th Annual Logging Symposium, 18–22 May 2014, Abu Dhabi, UAE.
Gharaibeh, A.A. 2017. *Environmental Impact Assessment on Oil Shale Extraction in Central Jordan*. PhD thesis, Technische Universitat Bergakademie Freiberg, Freiberg, Germany.
Golodkovskaia, G.A., Krasilova, N.S., Ladygin, V.M. and Shaumian, L.V. 1975. Factors controlling solid rock strength. *Bulletin of the International Association of Engineering Geology – Bulletin de l'Association Internationale de Géologie de l'Ingénieur*, **11**, 65–69, https://doi.org/10.1007/BF02635456
Goodway, B., Perez, M. and Varsek, J. 2010. Seismic petrophysics and isotropic–anisotropic AVO methods for unconventional gas exploration. *Leading Edge*, **29**, 1500–1508, https://doi.org/10.1190/1.3525367
Grieser, W.V. and Bray, J.M. 2007. Identification of production potential in unconventional reservoirs. Paper SPE-106623-MS presented at the Production and Operations Symposium, 31 March–3 April 2007, Oklahoma City, Oklahoma, USA, https://doi.org/10.2118/106623-MS
Grohmann, S., Gaus, G. *et al.* 2021. Hydrous pyrolysis of source rock plugs geochemical and visual investigations and implications for primary migration. *In*: *30th International Meeting on Organic Geochemistry (IMOG 2021)*. European Association of Geoscientists & Engineers (EAGE), Houten, The Netherlands, https://doi.org/10.3997/2214-4609.202134153
Gunsallus, K.L. and Kulhawy, F.H. 1984. A comparative evaluation of rock strength measures. *International Journal of Rock Mechanics and Mining Sciences & Geomechanics Abstracts*, **21**, 233–248, https://doi.org/10.1016/0148-9062(84)92680-9
Hakimi, M.H., Abdullah, W.H., Alqudah, M., Makeen, Y.M. and Mustapha, K.A. 2016. Organic geochemical and petrographic characteristics of the oil shales in the Lajjun area, Central Jordan: Origin of organic matter input and preservation conditions. *Fuel*, **181**, 34–45, https://doi.org/10.1016/j.fuel.2016.04.070
Haq, B. and Al-Qahtani, A. 2005. Phanerozoic cycles of sea level change on the Arabian Platform. *GeoArabia*, **10**, 127–160, https://doi.org/10.2113/geoarabia1002127
Herwanger, J.V., Bottrill, A.D. and Mildren, S.D. 2015. Uses and abuses of brittleness index with applications to hydraulic stimulation. *In*: *Proceedings of the Unconventional Resources Technology Conference, San Antonio, Texas, USA, 20–22 July 2015*. Society of Exploration Geophysicists (SEG), Houston, TX, 1215–1223, https://doi.org/10.15530/urtec-2015-2172545
Hetenyi, M.I. 1950. *Handbook of Experimental Stress Analysis*.John Wiley & Sons, New York.
Hooker, J.N. and Cartwright, J.A. 2016. Dolomite overgrowths suggest a primary origin of cone-in-cone. *Geological Magazine*, **155**, 568–585, https://doi.org/10.1017/S0016756816000807
Hooker, J.N., Huggett, J.M., Cartwright, J. and Ali Hussein, M. 2017. Regional-scale development of opening-mode calcite veins due to silica diagenesis. *Geochemistry, Geophysics, Geosystems*, **18**, 2580–2600, https://doi.org/10.1002/2017GC006888
Hooker, J.N., Abu-Mahfouz, I.S., Meng, Q. and Cartwright, J. 2019. Fractures in mudrocks: Advances in constraining timing and understanding mechanisms. *Journal of Structural Geology*, **125**, 166–173, https://doi.org/10.1016/j.jsg.2018.04.020
Horsund, P. 2001. Estimating mechanical properties of shale from empirical correlations. *SPE Drilling & Completion*, **16**, 68–73, https://doi.org/10.2118/56017-PA
Huggett, J., Hooker, J.N. and Cartwright, J. 2017. Very early diagenesis in a calcareous, organic-rich mudrock from Jordan. *Arabian Journal of Geosciences*, **10**, 1–12, https://doi.org/10.1007/s12517-017-3038-5
Hugman, R.H.H. and Friedman, M. 1979. Effects of texture and composition on mechanical behavior of experimentally deformed carbonate rocks. *AAPG Bulletin*, **63**, 1478–1489.
Ibrahim, K.M., Aljurf, S., Rahman, H.A. and Gulamber, C. 2019. Exploration and evaluation of oil shales resources from Attarat area, Central Jordan. *In*: Benzer, H., Aydoğan, N. *et al.* (eds) *IMCET 2019 – Proceedings of the 26th International Mining Congress and Exhibition of Turkey*. TMMOB Chamber of Mining Engineers, Ankara, 1116–1128.
Irfan, T.Y. 1996. Mineralogy, fabric properties and classification of weathered granites in Hong Kong. *Quarterly Journal of Engineering Geology and Hydrogeology*, **29**, 5–35, https://doi.org/10.1144/GSL.QJEGH.1996.029.P1.02
Jaber, J.O., Amri, A. and Ibrahim, K. 2011. Experimental investigation of effects of oil shale composition on its calorific value and oil yield. *International Journal of Oil, Gas and Coal Technology*, **4**, 307–321, https://doi.org/10.1504/IJOGCT.2011.043714
Jahandideh, A. and Jafarpour, B. 2016. Optimisation of hydraulic fracturing design under spatially variable shale fracability. *Journal of Petroleum Science and Engineering*, **138**, 174–188, https://doi.org/10.1016/j.petrol.2015.11.032
Khoury, H.N. 2015. Uranium minerals of central Jordan. *Applied Earth Science*, **2**, 104–128, https://doi.org/10.1179/1743275815Y.0000000005
Koncagül, E.C. and Santi, P.M. 1999. Predicting the unconfined compressive strength of the Breathitt shale using slake durability, Shore hardness and rock structural properties. *International Journal of Rock Mechanics and Mining Sciences*, **36**, 139–153, https://doi.org/10.1016/S0148-9062(98)00174-0
Lavina, B., Dera, P. and Downs, R.T. 2014. Modern X-ray diffraction methods in mineralogy and geosciences. *Reviews in Mineralogy and Geochemistry*, **78**, 1–31, https://doi.org/10.2138/rmg.2014.78.1
Li, K., Samara, H., Wang, X., Jaeger, P., Ganzer, L. and Wegner, J. 2019. Reservoir characteristics and resource potential of oil shale in Sultani area, central of Jordan. Paper SPE-197606-MS presented at the International Petroleum Exhibition & Conference, 11–14 November 2019, Abu Dhabi, UAE, https://doi.org/10.2118/197606-MS
Li, Y. and Wang, J. 2019. Effects of porosity of dry and saturated sandstone on the energy dissipation of stress wave. *Advances in Civil Engineering*, **2019**, 9183969, https://doi.org/10.1155/2019/9183969
Lopes, F.C. and Cunha, P.P. 2007. Tectono-sedimentary phases of the latest Cretaceous and Cenozoic compressive evolution of the Algarve margin (southern Portugal). *International Association of Sedimentologists Special Publications*, **38**, 111–136, https://doi.org/10.1002/9781444304411.ch6
Lovelock, P.E.R. 1984. A review of the tectonics of the northern Middle East region. *Geological Magazine*, **121**, 577–587, https://doi.org/10.1017/S0016756800030727
Luan, X., Di, B., Wei, J., Li, X., Qian, K., Xie, J. and Ding, P. 2014. Laboratory measurements of brittleness anisotropy in synthetic shale with different cementation. *In*: *Proceedings of the Society of Exploration Geophysicists International Exposition and 84th Annual Meeting (SEG Denver 2014)*. Society of Exploration Geophysicists (SEG), Houston, TX, 3005–3009.
Meehan, R.L., Dukes, M. and Shires, P.O. 1975. A case history of expansive claystone damage. *Journal of Geotechnical and Geoenvironmental Engineering*, **101**, 933–948, https://doi.org/10.1061/AJGEB6.0000197
Mews, K.S., Alhubail, M.M. and Barati, R.G. 2019. A review of brittleness index correlations for unconventional tight and ultra-tight reservoirs. *Geosciences*, **9**, 319, https://doi.org/10.3390/geosciences9070319
Murphy, E.E., Praznik, G., Quirein, J., Galford, E.J., Witkowsky, J.M. and Chen, S. 2013. A workflow to evaluate mineralogy, porosity, TOC, and hydrocarbon volume in the Eagle Ford Shale. Paper SPE-167012-MS presented at the SPE Unconventional Resources Conference and Exhibition – Asia Pacific, 11–13 November 2013, Brisbane, Australia, https://doi.org/10.2118/167012-MS

Noah, A. and Shazly, T. 2014. Integration of well logging analysis with petrophysical laboratory measurements for Nukhul Formation at Lagia-8 well, Sinai, Egypt. *American Journal of Research Communication*, **2**, 139–166.

Pan, X.-P., Zhang, G.-Z. and Chen, J.-J. 2020. The construction of shale rock physics model and brittleness prediction for high-porosity shale gas-bearing reservoir. *Petroleum Science*, **17**, 658–670, https://doi.org/10.1007/s12182-020-00432-2

Peters, K.E. and Cassa, M.R. 1994. Applied source rock geochemistry: Chapter 5: Part II. Essential elements. *AAPG Memoirs*, **60**, 93–120.

Powell, J.H. 1989. *Stratigraphy and Sedimentation of the Phanerozoic rocks in Central and South Jordan. Part B: Kurnub, Ajlun and Belqa Groups*. Geological Mapping Division Bulletin, **11**. Geological Directorate, Natural Resources Authority, Amman.

Powell, J.H. and Moh'd, B.K. 2011. Evolution of Cretaceous to Eocene alluvial and carbonate platform sequences in central and south Jordan. *GeoArabia*, **16**, 29–82, https://doi.org/10.2113/geoarabia160429

Powell, J.H. and Moh'd, B.K. 2012. Early diagenesis of Late Cretaceous chalk–chert–phosphorite hardgrounds in Jordan: implications for sedimentation on a Coniacian–Campanian pelagic ramp. *GeoArabia*, **17**, 17–38, https://doi.org/10.2113/geoarabia170417

Quennell, A.M. 1951. The geology and mineral resources of Trans-Jordan. *Colonial Geology and Mineral Resources*, **2**, 85–115.

Quirein, J.A., Murphy, E.E., Praznik, G., Witkowsky, J.M., Shannon, S. and Buller, D. 2012. A comparison of core and well log data to evaluate porosity, TOC, and hydrocarbon volume in the Eagle Ford Shale. Paper SPE-159904-MS presented at the SPE Annual Technical Conference and Exhibition, 8–10 October 2012, San Antonio, Texas, USA, https://doi.org/10.2118/159904-MS

Ramsey, J.G. 1967. *Folding and Fracturing of Rocks*. McGraw-Hill, London.

Richard, T., Dagrain, F., Poyol, E. and Detournay, E. 2012. Rock strength determination from scratch tests. *Engineering Geology*, **147–148**, 91–100, https://doi.org/10.1016/j.enggeo.2012.07.011

Rickman, R., Mullen, M.J., Petre, J.E., Grieser, W.V. and Kundert, D. 2008. A practical use of shale petrophysics for stimulation design optimization: All shale plays are not clones of the Barnett Shale. Paper SPE-115258-MS presented at the SPE Annual Technical Conference and Exhibition, 21–24 September 2008, Denver, Colorado, USA, https://doi.org/10.2118/115258-MS

Russell, B.H. and Smith, T. 2007. The relationship between dry rock bulk modulus and porosity – an empirical study. *CREWES Research Reports*, **19**, 1–14.

Schei, G., Fjær, E., Detournay, E., Kenter, C.J. and Zausa, F. 2000. The scratch test: An attractive technique for determining strength and elastic properties of sedimentary rocks. Paper Number: SPE-63255-MS presented at the SPE Annual Technical Conference and Exhibition, 1–4 October 2000, Dallas, Texas, USA, https://doi.org/10.2118/63255-MS

Sharma, R.K. and Chopra, S. 2012. New attribute for determination of lithology and brittleness. *SEG Technical Program Expanded Abstracts*, **2012**, 1–5, https://doi.org/10.1190/segam2012-1389.1

Sokol, E.V., Kozmenko, O.A. *et al.* 2017. Calcareous sediments of the Muwaqqar Chalk Marl Formation, Jordan: Mineralogical and geochemical evidences for Zn and Cd enrichment. *Gondwana Research*, **46**, 204–226, https://doi.org/10.1016/j.gr.2017.03.008

Sone, H. and Zoback, M.D. 2013. Mechanical properties of shale-gas reservoir rocks – Part 2: ductile creep, brittle strength, and their relation to the elastic modulus. *Geophysics*, **78**, D393–D402, https://doi.org/10.1190/geo2013-0051.1

Sone, H. and Zoback, M.D. 2014. Time-dependent deformation of shale gas reservoir rocks and its long-term effect on the in situ state of stress. *International Journal of Rock Mechanics and Mining Sciences*, **69**, 120–132, https://doi.org/10.1016/j.ijrmms.2014.04.002

Speight, J.G. 2019. *Handbook of Industrial Hydrocarbon Processes*. Elsevier, Amsterdam.

Steiner, S., Ahsan, S.A., Raina, I., Dasgupta, S. and Lis, G.L. 2016. Interpreting total organic carbon TOC in source rock oil plays. Paper SPE-183050-MS presented at the Abu Dhabi International Petroleum Exhibition & Conference, 7–10 November 2016, Abu Dhabi, UAE, https://doi.org/10.2118/183050-MS

Tarasov, B. and Potvin, Y. 2013. Universal criteria for rock brittleness estimation under triaxial compression. *International Journal of Rock Mechanics and Mining Sciences*, **59**, 57–69, https://doi.org/10.1016/j.ijrmms.2012.12.011

Tarrer, A. and Wagh, V. 1991. *The Effect of the Physical and Chemical Characteristics of the Aggregate on Bonding*. Strategic Highway Research Program, National Research Council, Washington, DC.

Terres, R., Pierpont, R., Omari, W., Al Najjar, I. and Neal, S. 2012. *Jordan Oil Shale Resource Evaluation*. Shell published presentation, Amman, Jordan, 16 October 2012.

Tissot, B.P. and Welte, D.H. 1984. Chapter 5. From kerogen to petroleum. *In*: *Petroleum Formation and Occurrence*. 2nd edn. Springer, Berlin, 160–198, https://doi.org/10.1007/978-3-642-87813-8_10

Vernik, L. and Liu, X. 1997. Velocity anisotropy in shales: a petrophysical study. *Geophysics*, **62**, 403–692, https://doi.org/10.1190/1.1444151

Vutukuri, V.S., Lama, R.D. and Saluja, S.S. 1974. *Handbook on Mechanical Properties of Rocks, Volume 1*. Trans Tech Publications, Clausthal, Germany.

Wang, F.P. and Gale, J.F. 2009. Screening criteria for shale-gas systems. *Gulf Coast Association of Geological Societies Transactions*, **59**, 779–793.

Wicaksono, A.N., Abu-Mahfouz, I.S., Idiz, E., Cartwright, J., Santamarina, J.C. and Vahrenkamp, V.C. 2022. Stress distribution around kerogen particles as a measure of the initiation of bitumen-filled microfractures in organic-rich source rocks. *Methods X*, **9**, 101817, https://doi.org/10.1016/j.mex.2022.101817

World Energy Council 2016. *World Energy Resources*. World Energy Council, London.

Ye, Y., Tang, S. and Xi, Z. 2020. Brittleness evaluation in shale gas reservoirs and its influence on fracability. *Energies*, **13**, 388, https://doi.org/10.3390/en13020388

Zou, C.N., Yang, Z. and Cui, J.W. 2012. Formation mechanism, geological characteristics and development strategy of nonmarine shale oil in China. *Petroleum Exploration and Development*, **40**, 15–27, https://doi.org/10.1016/S1876-3804(13)60002-6